63-3-4

AFCRL-63-103

403 785

INVESTIGATION OF THE ENERGY LEVELS OF MAGNETIC IONS IN THE COMPLEX METAL OXIDES, ESPECIALLY IN THE ORTHOFERRITES

Robert L. White

General Telephone and Electronics Laboratories, Inc.
1015 Corporation Way
Palo Alto, California

Contract No. AF 19(628)-387

Project No. 5621

Task No. 562104

FINAL REPORT

March 28, 1963

Prepared for

Air Force Cambridge Research Laboratories
Office of Aerospace Research
United States Air Force
Bedford, Massachusetts

AFCRL-63-103

INVESTIGATION OF THE ENERGY LEVELS OF MAGNETIC IONS IN THE COMPLEX METAL OXIDES, ESPECIALLY IN THE ORTHOFERRITES

Robert L. White

General Telephone and Electronics Laboratories, Inc.
1015 Corporation Way
Palo Alto, California

Contract No. AF 19(628)-387

Project No. 5621

Task No. 562104

FINAL REPORT

March 28, 1963

Prepared for

Air Force Cambridge Research Laboratories
Office of Aerospace Research
United States Air Force
Bedford, Massachusetts

Requests for additional copies by Agencies of the Department of Defense, their contractors, and other government agencies should be directed to the:

ARMED SERVICES TECHNICAL INFORMATION AGENCY
ARLINGTON HALL STATION
ARLINGTON 12, VIRGINIA.

All other persons and organizations should apply to the:

U. S. DEPARTMENT OF COMMERCE
OFFICE OF TECHNICAL SERVICES
WASHINGTON 25. D. C.

INVESTIGATION OF THE ENERGY LEVELS OF MAGNETIC IONS
IN THE COMPLEX METAL OXIDES, ESPECIALLY IN THE ORTHOFERRITES

DISTRIBUTION LIST

Code	Organization	No. of Copies
AF 5	AFMTC (AFMTC Tech. Library-MU-135) Patrick AFB, Florida.	1
AF 18	AUL Maxwell AFB, Alabama.	1
AF 32	OAR (RROS, Col. John R. Fowler) Tempo D 4th and Independence Ave., Washington 25, D.C.	1
AF 33	AFOSR, OAR (SRYP) Tempo D 4th and Independence Ave., Washington 25, D.C.	1
AF 43	ASD (ASAPRD - Dist) Wright-Patterson AFB, Ohio	1
AF 124	RADC (RAALD) Griffiss AFB, New York Attn: Documents Library	1
AF 139	AF Missile Development Center (MDGRT) Holloman AFB, New Mexico	1
AF 314	Hq. OAR (RROSP, Maj. Richard W. Nelson) Washington 25, D.C.	1
Ar 5	Commanding General USASRDL Ft. Monmouth, N.J. Attn: Tech. Doc. Ctr. SIGRA/SL-ADT	1
Ar 9	Department of the Army Office of the Chief Signal Officer Washington 25, D.C. Attn: SIGRD-4a-2	1
Ar 50	Commanding Officer Attn: ORDTL-012 Diamond Ordnance Fuze Laboratories Washington 25, D.C.	1

Ar 67	Redstone Scientific Information Center U.S. Army Missile Command Redstone Arsenal, Alabama	1
G 31	Office of Scientific Intelligence Central Intelligence Agency 2430 E Street, N.W. Washington 25, D.C.	1
G 2	ASTIA (TIPAA) Arlington Hall Station Arlington 12, Virginia	10
G 68	Scientific and Technical Information Facility Attn: NASA Representative (S-AK-DL) P.O. Box 5700 Bethesda, Maryland	1
G 109	Director Langley Research Center National Aeronautics and Space Administration Langley Field, Virginia	1
N 9	Chief, Bureau of Naval Weapons Department of the Navy Washington 25, D.C. Attn: DLI-31	2
N 29	Director (Code 2027) U.S. Naval Research Laboratory Washington 25, D.C.	2
I 292	Director, USAF Project RAND The Rand Corporation 1700 Main Street Santa Monica, California Thru: AF Liaison Office	1
M 6	AFCRL, OAR (CRXRA - Stop 39) L.G. Hanscom Field Bedford, Mass.	20
AF 253	Technical Information Office European Office, Aerospace Research Shell Building, 47 Cantersteen Brussels, Belgium	1
AR 107	U.S. Army Aviation Human Research Unit U.S. Continental Army Command P. O. Box 428, Fort Rucker, Alabama Attn: Maj. Arne H. Eliasson	1

G 8	Library Boulder Laboratories National Bureau of Standards Boulder, Colorado	2
M 63	Institute of the Aerospace Sciences, Inc. 2 East 64th Street New York 21, New York Attn: Librarian	1
M 84	AFCRL, OAR (CRXR, J. R. Marple) L. G. Hanscom Field Bedford, Massachusetts	1
N 73	Office of Naval Research Branch Office, London Navy 100, Box 39 F.P.O., New York, New York	5
U 32	Massachusetts Institute of Technology Research Laboratory Building 26, Room 327 Cambridge 39, Massachusetts Attn: John H. Hewitt	1
U 431	Alderman Library University of Virginia Charlottesville, Virginia	1
G 9	Defense Research Member Canadian Joint Staff 2450 Massachusetts Avenue, N.W. Washington 8, D.C.	1
AF 318	Aero Res. Lab. (OAR) AROL Lib. AFL 2292, Bldg. 450 Wright-Patterson AFB, Ohio	1
AF 3	Aeronautical Research Laboratories, OAR (ARX) Attn: Mr. Marshall Kreitman Solid State Physics Research Laboratory Wright-Patterson AFB, Ohio	1
	Hq. AFCRL, OAR (CRRCSP-3, Peter D. Gianino) L. G. Hanscom Field Bedford, Massachusetts	9

ABSTRACT

The allowed spin configurations in the rare earth orthoferrite have been derived on the basis of group theory and correlated with those actually observed. The susceptibilities and antiferromagnetic resonance modes of $YFeO_3$ have been calculated. The paramagnetic resonance spectra of Fe^{3+} and Gd^{3+} in $YAlO_3$ were measured and the spectra analyzed to give spin Hamiltonian parameters for these ions. The Fe^{3+} site was found to be nearly cubic, but the Gd^{3+} site was badly distorted. The spin Hamiltonian parameters were compared with crystal fields calculated on a point ion model using positional parameters measured not for $YAlO_3$ but for $GdFeO_3$. Poor agreement was found. Further evidence that the crystal fields are substantially different in the ortho-aluminates from the orthoferrites were obtained in the optical spectrum of Yb^{3+} in $YAlO_3$ and $YbFeO_3$. The Fe^{3+} - Yb^{3+} exchange was observed in the optical spectrum of Yb^{3+} in $YbFeO_3$. The exchange splittings were large, 6 to 10 cm^{-1}, although the Yb^{3+} and Fe^{3+} spins are at nearly right angles, indicating a large antisymmetric exchange. Further studies are suggested to illuminate the orthoferrite magnetic structure.

TABLE OF CONTENTS

LIST OF ILLUSTRATIONS

List of Illustrations

INVESTIGATION OF THE ENERGY LEVELS OF MAGNETIC IONS IN THE COMPLEX METAL OXIDES, ESPECIALLY IN THE ORTHOFERRITES

I. INTRODUCTION.

The rare earth orthoferrites are a family of mixed oxides of chemical formula $M^{I}M^{II}O_3$ which crystallize in a slightly distorted perovskite[1-8] form. M^{I} is typically a trivalent rare earth ion and M^{II} a trivalent transition metal ion, though variations from this typical form (involving, say, Ca and Ba substitution) have been studied.[9-13] We will, in this report, restrict our attention primarily to the cases where M^{I} is Y^{3+}, Gd^{3+} or Yb^{3+}, and M^{II} is Fe^{3+}, Al^{3+} or Ga^{3+}.

The rare earth orthoferrites are interesting magnetically because they are in many instances canted antiferromagnets.[14] The magnetic ions group into sublattice whose magnetization is equal and whose direction is nearly, but not quite exactly, antiparallel. There is therefore a small permanent magnetic moment due to the failure of the sublattice magnetizations to cancel fully. The "canting angle" is the angle which the magnetic sublattices make with a truly antiparallel configuration, and the origin, temperature dependence, etc. of the canting is of considerable physical interest.

In this report we will examine the spin configurations possible in the orthoferrites from both a macroscopic and microscopic point of view. The work reported is the initial portion of the work aimed at understanding the magnetic properties of these materials from an atomic point of view.

II. CRYSTAL STRUCTURE AND SPIN CONFIGURATION OF ORTHOFERRITES.

The crystal structure of the rare earth orthoferrites and their related compound, the orthoaluminates, orthogalliates, orthochromites, etc. have been studied in considerable detail by Geller[1-7] and associates in this country and by Bertaut[8] and associates in France. We have unit cell dimensions for a wide range of M^{I}- M^{II} combinations but have at present detailed lattice parameter information - e.g. exact oxygen positions - only for gadolinium orthoferrite.[6]

The orthoferrites and their isomorphs (we will use the term orthoferrite in this report as the generic term for the family) crystallize in the cubic perovskite structure or in two distorted modifications of the perovskite structure, one orthorhombic and one rhombohedral. The compounds of greatest interest to us, the iron-bearing rare earth orthoferrites, all crystallize in the orthorhombic structure[1] belonging to space group D_{2h}^{16} - Dbnm. There are four distorted perovskite pseudo-cells in an orthorhombic unit cell, giving four inequivalent iron sites and four inequivalent rare earth sites per unit cell. The orthorhombic unit cell is drawn in Fig. 1. The rare earth ions have been omitted in Fig. 1 to simplify the picture. The iron sites and rare earth sites of the unit cell are shown separately in Fig. 2 and 3, with certain additional notations which will be utilized later. The iron positions are special position (1/2, 0, 0; 1/2, 0, 1/2; 0, 1/2, 0; 0, 1/2, 1/2), but all oxygens and rare earth ions are displaced by as much as a few tenths of an Angstrom from the idealized sites drawn in Figs. 1

through 3. These distortions will be discussed later relevant to the paramagnetic resonance and optical absorption measurements.

One can tell a great deal about the allowed spin configurations of the orthoferrite on the basis of magnetic symmetry considerations. The magnetic groups are obtained by adding to the symmetry point group elements a time reversal operation, R, which reverses all angular moments and magnetic fields.

The orthorhombic space group D_{2h} to which the orthoferrites belong has the point symmetry group elements

$$E,\ C_{2x},\ C_{2y},\ C_{2z},\ I, \sigma_x, \sigma_y, \sigma_z. \qquad \text{II-1}$$

where

E is the identity operator

C_{2x}, C_{2y}, C_{2z} are rotations of π about the designated axes

I is the inversion operator

σ_x, σ_y, σ_z are reflection symmetry operations.

The addition of R, time reversal, to the point symmetry elements of a crystal containing angular momentum results in the generation of several magnetic groups. The point group itself remains a symmetry group and a number of additional groups are generated, each of which contains R in half its elements.

The orthorhombic group D_{2h} gives rise, in the presence of angular momenta, to the following magnetic groups:

(1)	E	I	C_{2x}	C_{2y}	C_{2z}	σ_x	σ_y	σ_z
(2)	E	I	C_{2x}	σ_x	RC_{2y}	RC_{2z}	$R\sigma_y$	$R\sigma_z$
(3)	E	I	C_{2z}	σ_z	RC_{2x}	RC_{2y}	$R\sigma_x$	$R\sigma_y$
(4)	E	I	C_{2y}	σ_y	RC_{2x}	RC_{2z}	$R\sigma_x$	$R\sigma_z$
(5)	E	C_{2x}	C_{2y}	C_{2z}	RI	$R\sigma_x$	$R\sigma_y$	$R\sigma_z$
(6)	E	C_{2x}	σ_y	σ_z	RI	RC_{2y}	RC_{2z}	$R\sigma_x$
(7)	E	C_{2y}	σ_x	σ_z	RI	RC_{2x}	RC_{2z}	$R\sigma_y$
(8)	E	C_{2z}	σ_x	σ_y	RI	RC_{2x}	RC_{2y}	$R\sigma_z$

II-2

We now look at the orthoferrite to see to which of these groups it may belong. The point group operations transform the various ion sites into one another, so we must first develop a scheme of labeling of the cation sites on which the angular momentum (spin) is located. We will use the scheme indicated in Figs. 2 and 3, which is consistent with the notation of Heeger[15] in his discussion of the isostructural $KMnF_3$, and of Treves[16] in his discussion of magnetic susceptibilities in the orthoferrites. The convention is similar for the iron and for the rare earth sites:

Horizontal nearest neighbors (1,4) (2,3)

Vertical nearest neighbors (1,2) (3,4)

Next-to-nearest neighbors (1,3) (2,4).

Table II-1 lists the possible permutations of the cation sites and gives the corresponding symmetry operations which produce them

Permutation	Fe	R.E.
Identity	E, I	E, σ_z
$1 \leftrightarrow 4$, $2 \leftrightarrow 3$	C_{2x}, σ_x	C_{2y}, σ_x
$1 \leftrightarrow 3$, $2 \leftrightarrow 4$	C_{2y}, σ_y	C_{2y}, σ_y
$1 \leftrightarrow 2$, $3 \leftrightarrow 4$	C_{2z}, σ_z	C_{2z}, I

TABLE II-1

We first note that the inversion operator, I, carries the iron sites back into themselves (without reversing angular momentum). The operation RI, which would map iron sites onto themselves and then reverse their angular momentum, therefore cannot be an element of the orthoferrite magnetic symmetry group. We therefore eliminate immediately magnetic symmetry groups 5 through 8 of II-2 for the orthoferrite. We can now deduce the spin configurations compatible with magnetic symmetry for groups 1 through 4, since we know both what the group operators do to the individual angular momenta and also what permutations are induced. For instance, denoting the Fe angular momenta by $\vec{S}_i$ ($i = 1, \ldots 4.$) and the rare earth angular momentum by J_i, we have

$$\begin{aligned} C_{2x}S_{1x} &= S_{1x} = S_{4x} \\ C_{2x}S_{1y} &= -S_{1y} = S_{4y} \\ C_{2x}S_{1z} &= -S_{1z} = S_{4z}. \end{aligned} \qquad \text{II-3}$$

Therefore any group containing element C_{2x} corresponds to a spin configuration with

$$S_{1x} = S_{4x},\ S_{1y} = -S_{4y},\ S_{1z} = -S_{4z} \qquad \text{II-4}$$

Similarly

$$\begin{aligned} (RC_{2x})S_{1x} &= -S_{1x} = S_{4x} \\ (RC_{2x})S_{1y} &= S_{1y} = S_{4y} \\ (RC_{2x})S_{1z} &= S_{1z} = S_{4z}; \end{aligned} \qquad \text{II-5}$$

so spin configurations corresponding to a magnetic group containing (RC_{2x}) will have

$$S_{1x} = -S_{4x} \quad S_{1y} = S_{4x} \quad S_{1z} = S_{4z}. \qquad \text{II-6}$$

Following this procedure one obtains the magnetic structure corresponding to each group. Before listing these configurations we further note one operator of special interest, σ_z, which transforms the rare earth sites into themselves. For groups containing σ_z,

$$\begin{aligned} \sigma_z J_{ix} &= -J_{ix} = J_{ix} \\ \sigma_z J_{iy} &= -J_{iy} = J_{iy} \\ \sigma_z J_{iz} &= J_{iz} = J_{iz}. \end{aligned} \qquad \text{II-7}$$

Hence

$$J_{ix} = J_{iy} = 0 \qquad \text{II-8}$$

in groups containing σ_z.

Collecting the results of such considerations one has the allowed configurations:

(1) E, I, C_{2x}, C_{2y}, C_{2z}, σ_x, σ_y, σ_z

Fe	R.E.
$S_{1x} = -S_{2x} = -S_{3x} = S_{4x}$	$J_{ix} = 0$
$S_{1y} = -S_{2y} = S_{3y} = -S_{4y}$	$J_{iy} = 0$
$S_{1z} = S_{2z} = -S_{3z} = -S_{4z}$	$J_{1z} = J_{2z} = -J_{3z} = -J_{4z}$

(2) E, I, C_{2x}, σ_x, RC_{2y}, $R\sigma_y$, RC_{2z}, $R\sigma_z$

Fe	R.E.
$S_{1x} = S_{2x} = S_{3x} = S_{4x}$	$J_{1x} = J_{2x} = J_{3x} = J_{4x}$
$S_{1y} = S_{2y} = -S_{3y} = -S_{4y}$	$J_{1y} = J_{2y} = -J_{3y} = -J_{4y}$
$S_{1z} = -S_{2z} = S_{3z} = -S_{4z}$	$J_{iz} = 0$

(3) E, I, C_{2z}, σ_z, RC_{2x}, RC_{2y}, $R\sigma_x$, $R\sigma_y$ II-9

Fe	R.E.
$S_{1x} = -S_{2x} = S_{3x} = -S_{4x}$	$J_{ix} = 0$
$S_{1y} = -S_{2y} = -S_{3y} = S_{4y}$	$J_{iy} = 0$
$S_{1z} = S_{2z} = S_{3z} = S_{4z}$	$J_{1z} = J_{2z} = J_{3z} = J_{4z}$

(4) E, I, C_{2y}, σ_y, RC_{2x}, $R\sigma_x$, RC_{2z}, $R\sigma_z$

Fe	R.E.
$S_{1x} = S_{2x} = -S_{3x} = -S_{4x}$	$J_{1x} = J_{2x} = -J_{3x} = -J_{4x}$
$S_{1y} = S_{2y} = S_{3y} = S_{4y}$	$J_{1y} = J_{2y} = J_{3y} = J_{4y}$
$S_{1z} = -S_{2z} = -S_{3z} = S_{4z}$	$J_{iz} = 0$

We have pursued the problem thus far with the only information input being the crystalline symmetry of the orthoferrite. We now inject a physical assumption concerning the magnetic structure, namely that the interaction between nearest neighbor iron ions be antiferromagnetic. S_2 and S_4 are then constrained to be essentially antiparallel to S_1 and S_3. We find that magnetic group 4 does not allow of such a configuration so we drop it from further consideration in this report on the antiferromagnetic orthoferrites. (It is however the appropriate group for certain ferromagnetic configurations in the orthochromite and orthomanganate family[9,10]). The other three groups give one pure antiferromagnetic and two canted antiferromagnetic configurations as follows

Magnetic Symmetry Group	Predominant Fe spin direction	Canting direction
1	y	None
2	z	x
3	x	z

TABLE II-2

All three configurations are actually found.[17] Type 3 is the commonest form; it is the spin configuration for yttrium orthoferrite at all temperatures, and of nearly all the rare earth orthoferrites at room temperature and above. At lower temperatures, usually below 100° K, many of the rare earth orthoferrites switch to configuration (2) and a few to configuration (1).

The stable configuration is probably determined by the anisotropies of the separate spin systems. If, for instance, the local crystal field effects were such that the iron ions in $YFeO_3$ occupied their lowest energy position when their spin was parallel to an orthorhombic a direction (x direction), configuration (3) would be preferred. If a y-directed spin gave lowest energy, the antiferromagnetic configuration (1) would be preferred, and so on. The paramagnetic resonance and optical absorption experiments reported below were instituted to establish these correlations, and the relationship of these spectra to the actual spin configurations will be discussed in section IV-C.

III. MAGNETIC SUSCEPTIBILITIES AND ANTIFERROMAGNETIC RESONANCE MODES.

Before proceeding to the atomic spectroscopy and its interpretation we shall first examine some of the more macroscopic magnetic properties of the orthoferrites. It is indeed from such macroscopic magnetic measurements,[17-21] plus some very elegant neutron diffraction experiments,[9-13] that we have most of our present information on the orthoferrites.

An extensive set of magnetic susceptibility measurements have been made by the Grenoble group in France[19,20] and by Bozorth[17,21] and associates at Bell Telephone Laboratories, though the bulk of the results have never been published in detail. The principal results may be summarized as follows.

The magnetization of the rare earth ferrites may be described by a permanent moment plus a susceptibility (much as for the garnets)

$$\sigma = \sigma_o + XH. \qquad \text{III-1}$$

The ferromagnetic (or permanent) component σ_o is about .05 Bohr magnetons per molecule at room temperature for all the rare earth orthoferrites. The direction of σ_o is always in either an orthorhombic c or orthorhombic a direction. For all of the crystals observed except $SmFeO_3$ the c axis is the direction of σ_o at room temperature. For an orthoferrite with a magnetically inactive rare earth (such as Y or La) the permanent moment σ_o remains essentially constant in magnitude and direction down to liquid Helium temperatures. For a rare earth orthoferrite containing a rare earth such as Holmium, Erbium, or Dysprosium the permanent moment increases substantially as the temperature is lowered, and σ_o usually flips to the

a direction or drops suddenly to zero at a transition temperature. Some exceptional behaviors appear; gadolinium with its large magnetic moment appears to act as if it were magnetically inert in the orthoferrite.

The general features of the magnetic behavior we can understand on the basis of our foregoing magnetic group theory, and by extrapolation from other magnetic materials, notably the garnets.[22]

Let us first assume that the iron ions are coupled antiferromagnetically with a strong interaction ($T_c \approx 680^\circ$ K). The rare earths are then coupled to the iron ions with a rather weak exchange ($T_K \approx 20^\circ$ K). At temperatures appreciably higher than T_K, such as room temperature, the rare earths are negligibly polarized by the exchange interaction, and σ_o is due primarily to the iron ions. We can account for the observed properties in this temperature region by assuming that the iron ions occupy the spin configuration given by magnetic group 3 of Table II-2. The iron ions then point predominantly in the plus and minus a (x) direction but are canted slightly in the z direction. A canting of about .01 radian would produce the moment observed; .05 Bohr magnetons per molecule out of a possible 5. As the temperature is lowered the weak rare-earth to iron exchange polarizes the rare earths more and more effectively, giving rise to an increasing σ_o. As the rare earths become more polarized, anisotropy effects arising in the rare earth ion lattice become more effective, and the whole magnetic structure can be flipped to that of magnetic groups No. 2 (Fe spins in $\pm$ z direction,

canted toward x) or to the antiferromagnetic configuration of symmetry group No. 1.

The general explanation raises a number of specific questions. For instance, why do the iron sublattices choose to cant with respect to one another? An isotropic exchange would cause the spins to minimize their energy by being rigorously antiparallel. The canting could be caused either by single ion anisotropy, or by antisymmetric exchange. The former is caused by the ions "feeling" the crystal lattice through crystalline electric field effects; the second is an exchange of the form $D \cdot S_1 \times S_2$ which tends to make the spins be perpendicular to each other. Dzialoshinski[23] and Moriya[24] have shown that such an interaction is allowed (on symmetry grounds) in the orthoferrite and have suggested an atomic mechanism for the interaction. Treves[16] has attempted to identify the canting mechanism on the basis of torque measurements and concludes that the antisymmetric exchange is responsible. We have come to substantially the same conclusion based on other arguments, detailed subsequently.

Let us first derive the magnetic susceptibility and magnetic resonant modes of the canted antiferromagnet. This calculation has been reported in detail in a scientific report, "Resonance and RF Susceptibilities in Orthoferrites" by G. F. Herrmann,[25] and we will only summarize the results here.

We restrict our attention first to the simplest case, $YFeO_3$, where the rare earth sites are occupied by non-magnetic ions. The appropriate

magnetic group is No. 3, the irons point predominantly in the x direction but are canted slightly in the z direction. There are two antiferromagnetic resonant modes of the system; ω_z, for which the precession ellipse of each sublattice magnetization is elongated in the xz plane; and ω_{xy}, for which precession ellipse is elongated in the xy plane.

We will derive the required properties from an expression for the free energy. It is convenient to express the energy in units of magnetic field. Defining

$$M = \left|\underset{\sim}{M}_1\right| = \left|\underset{\sim}{M}_2\right|, \qquad \text{III-2}$$

where $\underset{\sim}{M}_1$ and $\underset{\sim}{M}_2$ are the sublattice magnetization vectors pointing approximately in the plus and minus x directions respectively, we shall put

$$V = W/M, \qquad \text{III-3}$$

where W is the free energy. We shall then write W as a function of the unit vectors

$$R_1 = (x_1, y_1, z_1)$$
$$R_2 = (x_2, y_2, z_2), \qquad \text{III-4}$$

$$\underset{\sim}{R}_1 = \underset{\sim}{M}_1/M \text{ and } \underset{\sim}{R}_2 = \underset{\sim}{M}_2/M, \qquad \text{III-5}$$

and retain only quadratic terms in R_1 and R_2.

The most general form of the magnetic anisotropy tensor for M_1 allowed by symmetry considerations is then

$$-(A_{xx}x_1^2 + A_{zz}z_1^2 + A_{xz}x_1z_1), \qquad \text{III-6}$$

where A_{xx}, A_{zz}, and A_{xz} are macroscopic energy coefficients related to the crystal field splittings. Similarly the anisotropy tensor for M_2 is

$$-(A_{xx}\, x_2^2 + A_{zz}\, z_2^2 - A_{xz}\, x_2 z_2). \qquad \text{III-7}$$

The symmetric and antisymmetric exchange terms are given by

$$E\, \underset{\sim}{R}_1 \cdot \underset{\sim}{R}_2 \qquad \text{III-8}$$

and

$$-D\,(x_1 z_2 - x_2 z_1) \qquad \text{III-9}$$

respectively.

The normalized free energy of the system is then

$$\begin{aligned} V = {} & E(\underset{\sim}{R}_1 \cdot \underset{\sim}{R}_2) - D(x_1 z_2 - x_2 z_1) \\ & - A_{xx}(x_1^2 + x_2^2) - A_{zz}\,(z_1^2 + z_2^2) \\ & - A_{xz}\,(x_1 z_1 - x_2 z_2). \end{aligned} \qquad \text{III-10}$$

One then solves for the equilibrium position of M_1 and M_2, their normal modes of oscillation, and their perturbation by an external magnetic field. This is done in the report referenced above, and we shall list the important conclusions here.

We have for the magnetic susceptibilities

$$\begin{aligned} \sigma_x &= \chi_{xx} H_x + 2C_{xxz} H_x H_z \\ \sigma_y &= \chi_{yy} H_y \\ \sigma_z &= \sigma_{zo} + \chi_{zz} H_z + C_{xxz} H_x^2 \end{aligned} \qquad \text{III-11}$$

where

$$\chi_{xx} \approx \frac{(A_{xz} + D)^2 M}{4E\left[E(A_{xx} - A_{zz}) + A_{xz}(A_{xz} + D)\right]}$$

$$\chi_{yy} = \chi_{zz} \approx \frac{M}{E} \qquad \text{III-12}$$

$$\sigma_{zo} = \frac{M(A_{xz} + D)}{E}$$

$$C_{xxz} \approx \frac{(A_{xz} + D)\left[8E(A_{xx} - A_{zz}) + (A_{xz} + D)(3A_{xz} - D)\right]}{32E\left[E(A_{xx} - A_{zz}) + A_{xz}(A_{xz} + D)\right]^2} .$$

Certain approximations have been made in the above expressions which amount substantially to the assumption that the isotropic exchange energy is large compared to the other energies involved, and that the canting angles are small.

Since A_{xz}, a measure of the canting effect of single ion anisotropy, and D, the antisymmetric exchange parameter, enter the expressions for χ_{xx}, and σ_{zo} to first order in the same form, $(A_{xz} + D)$, it is not possible to determine these parameters separately from susceptibility measurements until one invokes a measurement of C_{xxz}, a very small higher order coefficient. Susceptibility measurements are therefore a poor tool for distinguishing these two effects analytically. However, the σ_{zo} measured implies that

$$\frac{A_{xz} + D}{E} \approx 10^{-2}, \qquad \text{III-13}$$

or that the "canting field" be approximately one one-hundreth of the exchange field. Since the equivalent exchange field is on the order of 10^7 oe., we

deduce that the "canting field," a fictitious field at right angles to the exchange field capable of producing the observed canting, must be on the order of 10^5 oe., which is one or two orders of magnitude greater than the anisotropy fields usually associated with the Fe^{3+} ions. (A more quantitative discussion of this is given below). We are therefore inclined by the susceptibility measurements to suspect antisymmetric exchange as the source of canting.

A better technique for separating out single ion anisotropy effects from antisymmetric exchange effects is offered by antiferromagnetic resonance. The two sublattice system has two resonance modes of frequency ω_z and ω_{xy} as mentioned above and described in the referenced report. In the absence of an external field the resonant frequencies are

$$\omega_z^2(0)/\gamma^2 = 4E(A_{xx} - A_{zz}) + 4A_{xx}(A_{xx} - A_{zz}) + 4A_{xz}(A_{xz} + D)$$

$$\omega_{xz}^2(0)/\gamma^2 = 4E(A_{xx}) + 4A_{xx}(A_{xx} - A_{zz}) + (A_{xz} + D)^2. \qquad \text{III-14}$$

The dominant term for both modes is the typical $\sqrt{H_e H_a}$ type term. For the orthoferrite $H_e \approx 10^7$ and $H_a \approx 10^3 \longrightarrow 10^5$ (guesses based on T_c and typical Fe^{3+} anisotropy fields) so the resonant frequency might fall at frequencies ranging from $\gamma \times 10^5$ (or 280 kMc) to $\gamma \times 3 \times 10^5$ (or 1,000 kMc). On the other hand, the $(A_{xx} - A_{zz})$ cancellation in the ω_z mode might bring the frequency downward to 100 kMc or less. Magnetic resonances of some sort were once seen in the orthoferrites by Dr. Simon Foner,[26] at the Lincoln Laboratories, at 70 kMc in magnetic fields ranging from a few kilogauss up to 120 kilogauss.

In the presence of magnetic fields the resonance frequencies become:

H_o in z direction (c axis)

$$\omega_z^2/\gamma^2 = \omega_z^2(0)/\gamma^2 + (A_{xz} + D)H_o \qquad \text{III-15}$$

$$\omega_{xy}^2/\gamma^2 = \omega_{xz}^2(0)/\gamma^2 + (5A_{xz} + D)H_o + H_o^2.$$

Expressions for ω_z, ω_{xy} with H_o in other directions are substantially more complicated and are given in the referenced report. One sees, however, that from the measurement of ω_z and ω_{xy} as a function of H_o, the single ion canting effect (measured by A_{xz}) and the antisymmetric exchange effect (measured by D) could be analytically separated.

We conducted a search for the antiferromagnetic resonance modes at frequencies from 55 to 65 kMc and in magnetic field up to 15 kilogauss. No resonances were observed. We conclude that our observation frequencies probably were not high enough. The closing of our laboratory precludes the extension of this search to higher frequencies within the present contract.

IV. PARAMAGNETIC RESONANCE: IRON

A. Experimental.

Yttrium orthoferrite is the simplest interesting orthoferrite, in the sense that it has only one kind of magnetically active ion present, trivalent iron. The magnetic properties of the yttrium orthoferrite are presumably fully determined by the nature of the ground state of the Fe^{3+} ion, by its interaction with its crystalline environment, and by its interaction with other Fe^{3+} ions.

The properties of the individual Fe^{3+} ion and its interaction with its crystalline environment can be determined through paramagnetic resonance spectroscopy. The ground state of the Fe^{3+} ion is a spectroscopic ^6S state, with $L = 0$ and $S = 5/2$. Since it is an S state its charge cloud is essentially spherically symmetric, and its energy of interaction with the crystalline electric potentials small, typically a few tenths of a wave number, (or a few tens of kilomegacycles). To study the isolated ion it must be substituted dilutely into a diamagnetic isomorph of the crystal of magnetic interest. We have used $YAlO_3$, yttrium orthoaluminate, for our host crystal[27] in the paramagnetic and optical studies. $YGaO_3$ would have been a more ideal diamagnetic host since trivalent gallium and trivalent iron have nearly the same radius, whereas aluminum is substantially smaller. However, $YGaO_3$ has never been reported as a stable phase, and all our attempts to grow $YGaO_3$ were unsuccessful (resulting usually in the garnet structure $Y_3Ga_5O_{12}$).

A substantial portion of the report period was in fact devoted to the problem of growing single untwinned crystals of $YAlO_3$. After some considerable exploratory work it was found that a melt containing 2 mole percent Al_2O_3, 2 mole percent Y_2O_3, 88 mole percent PbO and 8 mole percent PbF_2 could be made to yield regularly crystals approximately 2 mm on a side. However, these crystals were found to be almost invariably multiply twinned. Since small additions of SiO_2 had been previously found to affect substantially the growth habit of the aluminum garnets, a small addition of SiO_2 to the melt was tried, and an addition of approximately 1 mole percent of SiO_2 was found to suppress the twinning strongly. Spectrographic analysis has shown that the Si does not enter the orthoaluminate crystal in the process of modifying the growth habit; the Si content of $YAlO_3$ grown from SiO_2 doped melts and undoped melts was substantially the same. The crystals used throughout the paramagnetic resonance studies described below were grown from the melt composition described above, plus appropriate Fe^{3+}, Gd^{3+}, or Yb^{3+} dopings.

The paramagnetic resonance studies were performed primarily on a 35 kMc superheterodyne, magnetic resonance spectrometer. Most of the data were taken at liquid nitrogen temperatures, with a few measurements at 4.2° K. The Fe^{3+} site in the orthoferrite is of low symmetry, having only the inversion symmetry. Since there are four magnetically inequivalent iron sites per unit cell, and five transitions (of $\Delta M_z = 1$ type) per ion, one expects the principal spectrum to consist of 20 absorptions for a general orientation of the external magnetic field, H_o. For H_o

in the principal planes of the crystal (e.g. the ab plane) the number of magnetically inequivalent sites is reduced to two, and along the a, b, or c axes the iron sites are all magnetically equivalent.

The iron in the orthoaluminate is octahedrally coordinated, that is, has six oxygen nearest neighbors in a nearly cubical array. The oxygens are all displaced from their true cubic positions by amounts of a few tenths of an Angstrom[6] out of an ion separation of approximately two Angstroms. The position of ions is described more fully in the crystal field calculation of section IV-C. For present purposes it is sufficient to note that the low symmetry of the site means that one has no a priori knowledge of the orientation of the principal axes of the crystal field distortions, and indeed no guarantee that there would be any simple relationship between the principal axes of the quadratic potential and those of the biquadratic (fourth power) potential.

The paramagnetic resonance absorption spectrum of the Fe^{3+} ion in $YAlO_3$ was first recorded for H_o in the a-b plane and for H_o in the b-c plane. These data are presented in Figs. 4 and 5. It is not obvious from these data that any principal axes were intercepted. However, the extremal spacings of the outermost transitions at about 25^o from the b axis in the a-b plane, and the near symmetry in the spacings of a group of five lines at this orientation (the five transitions identified as sites 1 and 2 in Fig. 4), suggested that this direction was nearly a principal direction of the dominant perturbation. We expected the dominant perturbation to be quadratic in the spin components, as is usually the

case for the Fe^{3+} spectrum. We therefore took data with H_o in a plane containing the c axis and the extremum in the a-b plane. These data showed that the extremum was located in, or within two or three degrees of, the a-b plane. Concluding then that this direction, 25^o from b in the a-b plane, was a principal axis of the quadratic energy tensor, we took data with H_o in the plane perpendicular to this direction (henceforth called direction 3) and obtained the spectrum shown in Fig. 6.

B. Determination of the Spin Hamiltonian.

The fitting of the spin Hamiltonian for a spin 5/2 or 7/2 particle to the experimental data for a low symmetry site presents a formidable problem. In the present instance the iron site has only inversion symmetry; we can from this information eliminate only terms in the potential which correspond to $Y_\ell^m(\theta\phi)$ where m is odd. We have therefore Y_2^0, $Y_2^{\pm 2}$, Y_4^0, $Y_4^{\pm 2}$ and $Y_4^{\pm 4}$ terms remaining, and no a priori knowledge of the principal axes of the quadratic terms or the relationship these axes bear to the axes in which the fourth order potential takes its simplest form. Each guess at the eight constants in the spin Hamiltonian leads to a 6 x 6 matrix for each site, to be diagonalized at each H_o orientation for comparison with the experimental data. The labor involved in such a trial and error fitting is enormous, even with inspired guessing, and convergence of the procedure is in no way guaranteed.

It was necessary, therefore, to develop an analytic attack which circumvented the necessity for repeated diagonalization of the energy matrix. This attack proceeds as follows and on the principles outlined in the next paragraphs.

The ground state energy level of a paramagnetic S state ion in an external field is customarily given in terms of a spin Hamiltonian of the form

$$\mathcal{H} = g\beta \vec{H} \cdot \vec{S} + \mathcal{H}_a(\vec{S}). \qquad \text{IV-1}$$

The first term gives the Zeeman energy of interaction with the external field, and $\mathcal{H}_a(\vec{S})$ is the anisotropy energy which depends essentially on the orientation of the spin vector $\vec{S}$ with respect to the crystalline axes. For an S state ion, g can be assumed to be isotropic and have the value 2. The procedure below could be generalized to an anisotropic g but there is no merit for our present purposes in so doing.

One wishes to determine $\mathcal{H}_a(\vec{S})$ from the paramagnetic resonance experiments. If the Zeeman energy of $g\beta\vec{H} \cdot \vec{S}$ is sufficiently large, all off-diagonal elements of $\mathcal{H}_a$ will have negligible effect on the spectrum, and $\mathcal{H}_a$ can be deduced from consideration of the diagonal matrix elements only, without further attention to the off diagonal terms. In the present case, however, $\mathcal{H}_a$ is not negligible with respect to $g\beta H$ so a more elaborate analytic technique is involved. We shall show, however, that it is possible, from symmetry considerations, to process out of the data the effect of the off-diagonal elements, and again extract the full properties of $\mathcal{H}_a$ from the diagonal elements alone.

It is convenient to define from the outset two sets of coordinate systems; the first, denoted by subscripts 1, 2 and 3, being fixed in the crystal with respect to the given ion site, and the second,

denoted by x, y, z, such that z coincides with the applied field $\vec{H}$. $\mathcal{H}_a$ is usually given as a power series in the spin components S_1, S_2 and S_3. We shall put

$$\mathcal{H}_a = g\beta \sum_e V_\ell \, (S_1, S_2, S_3), \qquad \text{IV-2}$$

where V_ℓ are polynomials of order ℓ in the spin components, and the factor $g\beta$ has been included to give $\mathcal{H}_a$ in units of magnetic field, as is common.

For the purpose of our analysis it is important to construct the V_ℓ as operator equivalents[28-33] of harmonic polynomials of order ℓ in the directional cosines of some suitable radius vector. This can always be accomplished by the addition of certain spherically symmetric terms to any of the polynomials V_ℓ or their operator equivalents. Once written in this form, V_ℓ can be expressed as a sum of spherical harmonic functions Y_ℓ^m in any coordinate system, since for any fixed ℓ the Y_ℓ^m transform only among themselves in any orthogonal coordinate transformation. In the paramagnetic case the V_ℓ are real and symmetric in the variables. For any given value of S one need consider only terms with $\ell \leq 2S$.

We now apply 2nd order perturbation theory, assuming $\mathcal{H}_a$ small compared to $g\beta H$. Quantizing along the z direction one can write the following expression for the energy levels:

$$W(M_s) = g\beta H M_s + \langle M_s | \mathcal{H}_a | M_s \rangle + \sum_{M_s'} \frac{\langle M_s | \mathcal{H}_a | M_s' \rangle^2}{(M_s - M_s')g\beta H} . \qquad \text{IV-3}$$

Consider first the diagonal term $< M_s \mid \mathcal{H}_a \mid M_s >$. We expand each polynomial V_ℓ in terms of operator equivalents of the spherical harmonics in the (x,y,z) system

$$V_\ell (S_1, S_2, S_3) = \sum_m A_\ell^m Y_\ell^m (S_x, S_y, S_z). \qquad \text{IV-4}$$

Since this expansion involves a transformation from the (123) to the (xyz) system, the coefficients A_ℓ^m are functions of the orientation of $\vec{H}$ or

$$A_\ell^m = A_\ell^m (\alpha_1, \alpha_2, \alpha_3) \qquad \text{IV-5}$$

where $\vec{\alpha}$ represents a unit vector along $\vec{H}$. The diagonal matrix elements of V_ℓ are given by

$$< M_s \mid V_\ell \mid M_s > = A_\ell^o < M_s \mid Y_\ell^o \ (S) \mid M_s > \qquad \text{IV-6}$$

since for $m \neq 0$ $Y_\ell^m (\vec{S})$ has no diagonal elements. To obtain the angular dependence of A_ℓ^o, one substitutes the directional cosines α_i of $\vec{H}$ for S_i in Eq. (IV-5)*. In the (xyz) system one has, by definition, $\alpha_x = \alpha_y = 0$, $\alpha_z = 1$. Therefore, since, $Y_\ell^m (0,0,1) = 0$ for all $m \neq 0$

$$A_\ell^o = \frac{V_\ell (\alpha_1 \alpha_2 \alpha_3)}{Y_\ell^o (0,0,1)} \qquad \text{IV-7}$$

---

* When substituting α_i for S_i and vice versa, one must replace any polynomial in α_i by its proper operator equivalent. In this sense, any equation satisfied by α_i is also satisfied by S_i and vice versa.

and (IV-6) becomes

$$< M_s \mid V_\ell \mid M_s > = \frac{V_\ell (\alpha_1\alpha_2\alpha_3) < M_s \mid Y_\ell^o \mid M_s >}{Y_\ell^o (0,0,1)} . \qquad \text{IV-8}$$

The angular dependence of the diagonal matrix elements of V_ℓ is thus given, apart from numerical factors, by the "classical" expression $V_\ell (\alpha_1\alpha_2\alpha_3)$. The spectrum is thus the product of two parts. One, $< M_s \mid Y_\ell^o \mid M_s >$, gives the fixed structure of the spectrum as determined by the quantum numbers. The other is a scaling factor $V_\ell (\alpha_1\alpha_2\alpha_3)$ which depends only on the orientation of $\vec{H}$.

We give in Table IV-1 a list of a few of the more useful polynomials and their operator equivalents: consider for example a spin Hamiltonian term of the form

$$V_2(\vec{S}) = D\left[S_3^2 - \tfrac{1}{3} S(S+1)\right] + E(S_1^2 - S_2^2) \qquad \text{IV-9}$$

one then has

$$V_2(\alpha) = D(\alpha_3^2 - \tfrac{1}{3}) + E(\alpha_1^2 - \alpha_2^2) \qquad \text{IV-10}$$

and, making use of Table IV-1 and Eq. (IV-8),

$$< M_s \mid V_2 \mid M_s > = \tfrac{3}{2}\left[D(\alpha_3^2 - \tfrac{1}{3}) + E(\alpha_1^2 - \alpha_3^2)\right] x \left[M_s^2 - \tfrac{1}{3} S(S+1)\right] . \qquad \text{IV-11}$$

The problem of finding the spin Hamiltonian has thus been reduced to finding the orientation dependence of $< M_s \mid V_\ell \mid M_s >$.

$$Y_2^{\circ}(\vec{\alpha}) = \alpha_3^2 - \frac{1}{3}$$

$$< M_s \,|Y_2^{\circ}|\, M_s > = M_s^2 - \frac{1}{3} S(S+1)$$

$$Y_4^{\circ}(\vec{\alpha}) = \frac{1}{120} \left[35\, \alpha_3^4 - 30\alpha_3^2 + 3\right]$$

$$< M_s \,|Y_4^{\circ}|\, M_s > = \frac{1}{120} \left[35\, M_s^4 - 30S\,(S+1)M_s^2 + 25M_s^2 - 6S(S+1) + 3S^2(S+1)^2\right]$$

$$Y_6^{\circ}(\vec{\alpha}) = \frac{1}{2520} \left[231\, \alpha_3^6 - 315\, \alpha_3^4 + 105\, \alpha_3^2 - 5\right]$$

$$< M_s \,|Y_6^{\circ}|\, M_s > = \frac{1}{2520} \left[231\, M_s^6 - 315S(S+1)M_s^4 + 735M_s^4 + 105S^2(S+1)^2M_s^2 - 525S(S+1)M_s^2 + 294M_s^2 - 5S^3(S+1)^3 + 40S^2(S+1)^2 - 6S(S+1)\right]$$

$$V_{cub}(\vec{\alpha}) = \frac{1}{6} \left[\alpha_1^4 + \alpha_2^4 + \alpha_3^4 - \frac{3}{5}\right]$$

$$V_{cub}(\vec{S}) = \frac{1}{6} \left[S_1^4 + S_2^4 + S_3^4 - \frac{1}{5} S(S+1)\,(3S^2 + 3S - 1)\right] .$$

Also

$$Y_2^{\circ}(0,0,1) = \frac{2}{3}$$

$$Y_4^{\circ}(0,0,1) = \frac{1}{15}$$

$$Y_6^{\circ}(0,0,1) = \frac{2}{315}$$

TABLE IV-1

The next step involves the extraction of $< M_s \mid V_\ell \mid M_s >$ from the experimental data, by eliminating the contributions due to off-diagonal matrix elements. This is made possible by the following symmetry considerations. Suppose that we reverse the signs of M_s and M_s' in Eq. (IV-3). Since $< M_s \mid \mathcal{H}_a \mid M_s >$ and $|< M_s \mid \mathcal{H}_a \mid M_s' >|^2$ do not change sign, one finds

$$W(-M_s) = - g\beta H M_s + < M_s \mid \mathcal{H}_a \mid M_s > - \sum_{M_s'} \frac{|< M_s \mid \mathcal{H}_a \mid M_s' >|^2}{(M_s - M_s')g\beta H} \qquad \text{IV-12}$$

and, hence, the sum $W(M_s)+W(-M_s)$ is in first order independent of the off-diagonal terms. By using proper linear combinations of the transition frequencies one can thus eliminate the off-diagonal contribution and determine separately the orientation dependence of each V_ℓ. For any value of S, there are always exactly enough transitions to make such a determination complete.

Let us now turn explicitly to the solution of the Fe^{3+} spectrum. For Fe^{3+}, $S = \frac{5}{2}$ and $\mathcal{H}_a$ is given by

$$\mathcal{H}_a = g\beta V_2(\vec{S}) + g\beta V_4(\vec{S}). \qquad \text{IV-13}$$

The energy levels can be written out according to Eq. IV-3. The diagonal part $< M_s \mid \mathcal{H}_a \mid M_s >$ is found from Eq. IV-8, using values for $< M_s \mid Y_2^o \mid M_s >$ and $< M_s \mid Y_4^o \mid M_s >$ which can be found in the literature.[33] According to standard practice, each transition is characterized in terms of the magnetic field for which it is observed at a given fixed frequency ν_o. The five transitions, $M_s = -\frac{5}{2} \rightarrow -\frac{3}{2}$, $-\frac{3}{2} \rightarrow -\frac{1}{2}$, $-\frac{1}{2} \rightarrow \frac{1}{2}$, $\frac{1}{2} \rightarrow \frac{3}{2}$, $\frac{3}{2} \rightarrow \frac{5}{2}$,

occur at magnetic field values denoted respectively by H_1, H_2, H_3, H_4 and H_5. One obtains

$$H_1 = H_o + 4A_2^o + 2A_4^o + \Delta_1$$

$$H_2 = H_o + 2A_2^o - \frac{5}{2} A_4^o + \Delta_2$$

$$H_3 = H_o + \Delta_3 \qquad \text{IV-14}$$

$$H_4 = H_o - 2A_2^o + \frac{5}{2} A_4^o + \Delta_4$$

$$H_5 = H_o - 4A_2^o - 2A_4^o + \Delta_5$$

where $H_o = h\nu_o/g\beta$, and where Δ_i represent contributions arising from the off-diagonal matrix elements of $\mathcal{H}_a$. From IV-3 and IV-12 it follows that $\Delta_1 = \Delta_5$ and $\Delta_2 = \Delta_4$, provided H_o is substituted for H in the denominator of the off-diagonal contribution in the above equations. (This substitution in fact tends to improve the approximation.) One can now solve (IV-14) to give

$$A_2^o = \frac{1}{56}\left[5(H_1 - H_5) + 4\,(H_2 - H_4)\right] \qquad \text{IV-15}$$

$$A_4^o = \frac{1}{14}\left[H_1 - H_5 - 2(H_2 - H_4)\right].$$

We now apply this analysis specifically to the spectrum of Fe^{3+} in the orthoaluminate as plotted in Figs. 4, 5 and 6. First one decides on the basis of intuition and general morphology which five transitions or groups of five transitions belong to the same site for any one orientation of H_o. The grouping is indicated on the Figs. 4, 5 and 6. One then extracts

the parameter A_2^o and A_4^o for each orientation of the magnetic field. These are plotted in Figs. 7 and 8. There is one set of axes 1, 2, 3 and two crystal field parameters, D and E, such that all the points on the A_2^o curve can be fit to the expression

$$A_2^o = 3/2 \left[D(\alpha_3^2 - \tfrac{1}{3}) + E(\alpha_1^2 - \alpha_2^2)\right] . \qquad \text{IV-16}$$

A best fit to the data was obtained with D = - 1.45 kilo-oersted, E = 0.30 kilo-oersted, and the 1,2,3 axes (for a particular site) are defined by the following transformation upon the orthorhombic axes, a,b,c*

$$\begin{pmatrix} 1 \\ 2 \\ 3 \end{pmatrix} = \begin{pmatrix} -\cos 22^o \sin 38^o & \sin 22^o \sin 38^o & \cos 38^o \\ \cos 22^o \cos 38^o & -\sin 22^o \cos 38^o & \sin 38^o \\ \sin 22^o & \cos 22^o & 0 \end{pmatrix} \begin{pmatrix} a \\ b \\ c \end{pmatrix} \qquad \text{IV-17}$$

$$= \begin{pmatrix} -.570 & .231 & .788 \\ .730 & -.295 & .616 \\ .375 & .927 & 0 \end{pmatrix} \begin{pmatrix} a \\ b \\ c \end{pmatrix}$$

The angular variation of A_2^o in each of the experimental configurations was calculated using the above parameters and axes, and is plotted as the theoretical curve in Fig. 7. The closeness of the fit indicates the accuracy of the best fit solution.

The term in the Hamiltonian quadratic in the spins is therefore

$$V_2(\vec{S}) = -1.45 \left[S_3^2 - \tfrac{1}{3}S(S+1)\right] + 0.30 \left[S_1^2 - S_2^2\right] \qquad \text{IV-18}$$

---

* For the purpose of this transformation we regard 1, 2, 3 and a,b,c as unit vectors in their respective directions.

where S_1, S_2 and S_3 are the spin components in directions 1, 2 and 3 above. Expressed somewhat differently for subsequent comparison with the crystal field calculation, $V_2(\vec{S})$ may be written

$$V_2(\vec{S}) = D_1 S_1^2 + D_2 S_2^2 + D_3 S_3^2 \qquad \text{IV-19}$$

with $D_1 = +1.18$, $D_2 = 0.27$ and $D_3 = -1.45$ kilo-oersted.

We turn now to the term in $\mathcal{H}_a$ biquadratic in the spins, V_4. This term, in its full generality, contains nine independent parameters, and a complete determination of all these parameters from the spectrum is not feasible. We will make some simplifying assumptions concerning the fourth order terms and let the fit resulting be a test of the validity of the assumptions.

The simplifying assumption consists of assuming that V_4 has cubic symmetry. The Fe^{3+} is indeed surrounded by 6 O^{2-} ions which form a slightly distorted octahedron as is shown in Fig. 9. The coordination octahedron is tilted and rotated by substantial angles (circa 15°) from the coordination octahedron of the cubic perovskite, but the radius vectors to the O^{2-} are still nearly orthogonal to one another and of nearly equal length (c.f. equations VI-1, section VI-A)

We therefore take $V_4(\vec{S})$ to be of the form

$$V_4(\vec{S}) = aV_{cubic} = \frac{a}{6}\left[S_\xi^4 + S_\eta^4 + S_\zeta^4 - \frac{1}{5}S(S+1)(3S^2+3S-1)\right] \qquad \text{IV-20}$$

in the appropriate coordinate frame ξ, η, ζ. It then follows, from IV-7 that

$$A_4^{\circ}(\alpha_\xi, \alpha_\eta, \alpha_\zeta) = \frac{15a}{6}\left[\alpha_\xi^4 + \alpha_\eta^4 + \alpha_\zeta^4 - \frac{3}{5}\right] = a(1-5\phi) \qquad \text{IV-21}$$

where

$$\phi = \alpha_\xi^2 \alpha_\eta^2 + \alpha_\eta^2 \alpha_\zeta^2 + \alpha_\zeta^2 \alpha_\xi^2 \,. \qquad \text{IV-22}$$

Next, one attempts to fit the data points of Fig. 8 with a value of a and a choice of axes. The theoretical curves of Fig. 8 were plotted for a = -.035 Koe. and a coordinate frame ξ, η, ζ obtained from the orthorhombic axes by the transformation*

$$\begin{pmatrix} \xi \\ \eta \\ \zeta \end{pmatrix} = \begin{pmatrix} .807 & -.574 & .122 \\ .565 & .819 & .122 \\ -.174 & -.052 & .985 \end{pmatrix} \begin{pmatrix} a \\ b \\ c \end{pmatrix} . \qquad \text{IV-23}$$

The generally good fit can be taken as a confirmation of the approximation and of the fit parameters.

It is interesting to compare the axes of the cubic potential with the radius vectors, r_i, to the ligating oxygens. To do this we compare IV-23 with the direction cosines* of the r_i:

$$\begin{pmatrix} r_4 \\ r_6 \\ r_1 \end{pmatrix} = \begin{pmatrix} .772 & -.620 & .187 \\ .577 & .794 & .196 \\ -.139 & -.088 & .990 \end{pmatrix} \begin{pmatrix} a \\ b \\ c \end{pmatrix} \qquad \text{IV-24}$$

One sees that the axes of the cubic potential do indeed point essentially toward the oxygen neighbors.

---

* We again regard ξ, η, ζ, r_i, and a,b,c as unit vectors here.

The sign of $\underline{a}$ deduced here is negative; its sign relative to D can be deduced from the spectrum and the sign of D can be deduced from the temperature dependence of absorption intensities. The negative sign of $\underline{a}$ is in contradiction with Geschwind's[34] general conclusion on the sign of $\underline{a}$ for Fe^{3+} in octahedral coordination, but the experimental evidence seems conclusive in this case.

V. PARAMAGNETIC RESONANCE: GADOLINIUM.

A. Experimental.

The paramagnetic resonance experiments on Gd^{3+} in $YAlO_3$ were performed in substantially the same manner as those on Fe^{3+} in $YAlO_3$. The spectrometer frequency was approximately 35 kMc, and most of the experiments were done at liquid nitrogen temperatures.

The rare earth ion site in the orthoferrite is in a mirror plane perpendicular to the c axis. Therefore one principal axis of the relevant potential will always be the c axis, and the other axes are confined to the a-b plane. Further, the rare earth sites are coupled in pairs by an inversion through the iron sites, so there are only two magnetically inequivalent rare earth sites for the general orientation of H_o. For H_o in the b-c or a-c planes the four sites are all magnetically equivalent. The Gd^{3+} spectrum is therefore relatively more simple than the Fe^{3+} spectrum, even though there is a larger number of transitions per site (seven transitions of $\Delta M_z = \pm 1$) because of the larger spin, $S = 7/2$, of the Gd^{3+} ion.

The paramagnetic resonance absorption spectrum of Gd^{3+} with H_o in the a-b plane is plotted in Fig. 9. The absorption spectrum with H_o in the b-c plane is plotted in Fig. 10. All necessary information is contained in these two spectra.

B. Determination of the Spin Hamiltonian.

The same general procedures and philosophy that were used in solving the Fe^{3+} spectrum will be followed again in the resolving of the

Gd^{3+} spectrum. The angular behavior of the diagonal elements of the spin Hamiltonian will be used to derive information on the full spin Hamiltonian, including off-diagonal elements.

Since the spin of Gd^{3+} in 7/2, one must include also a term $V_6(\vec{S})$ in the spin Hamiltonian. There will now be seven transitions $M_s = -7/2 \rightarrow -\frac{5}{2}, -\frac{5}{2} \rightarrow -\frac{3}{2}, -\frac{3}{2} \rightarrow -\frac{1}{2}, -\frac{1}{2} \rightarrow \frac{1}{2}, \frac{1}{2} \rightarrow \frac{3}{2}, \frac{3}{2} \rightarrow \frac{5}{2}, \frac{5}{2} \rightarrow \frac{7}{2}$, which occur respectively at the magnetic field values H_1, H_2, H_3, H_4, H_5, H_6, H_7. One finds:

$$
\begin{aligned}
H_1 &= H_o + 6A_2^o + 10\,A_4^o + 3\,A_6^o + \Delta_1 \\
H_2 &= H_o + 4A_2^o + 5\,A_4^o - 7\,A_6^o + \Delta_2 \\
H_3 &= H_o + 2A_2^o - 6A_4^o + 7A_6^o + \Delta_3 \\
H_4 &= H_o + \Delta_4 \\
H_5 &= H_o - 2A_2^o + 6A_4^o + 7A_6^o + \Delta_5 \\
H_6 &= H_o - 4A_2^o + 5A_4^o + 7A_6^o + \Delta_6 \\
H_7 &= H_o - 6A_2^o - 10A_4^o - 3A_6^o + \Delta_7 .
\end{aligned}
\qquad \text{V-1}
$$

Again, for the off-diagonal contributions one has, to first order, $\Delta_1 = \Delta_7$, $\Delta_2 = \Delta_6$, $\Delta_3 = \Delta_5$ and one can solve the equations to give

$$
\begin{aligned}
A_2^o &= \frac{1}{168}\left[7(H_1 - H_7) + 8\,(H_2 - H_6) + 5(H_3 - H_5)\right] \\
A_4^o &= \frac{1}{308}\left[7(H_1 - H_7) - 6\,(H_2 - H_6) - 9(H_3 - H_5)\right] \\
A_6^o &= \frac{1}{132}\left[(H_1 - H_7) - 4\,(H_2 - H_6) + 5(H_3 - H_5)\right] .
\end{aligned}
\qquad \text{V-2}
$$

The spectra of Figs. 9 and 10 were processed to yield the angular forms of A_2^o, A_4^o and A_6^o in the a-b and b-c planes and the reduced data for A_2^o and A_4^o are plotted in Figs. 11 and 12 respectively. The variation and magnitudes of the A_6^o values were within the experimental scatter of the data, so the A_6^o information was not regarded as meaningful.

We have taken the c axis to be the z or distinct axis for the various terms in the spin Hamiltonian, since the symmetry of the site makes this a unique axis. We can then fit the A_2^o angular dependence to

$$A_2^o = \frac{3}{2}\left[D(\alpha_c^2 - 1/3) + E(\alpha_1^2 - \alpha_2^2)\right], \qquad \text{V-3}$$

where $D = +0.10$ Koe.

$E = -0.35$ Koe. V-4

The principal axes 1 and 2 are derived from the crystallographic a and b axes by a clockwise rotation of 28° about the +c direction. This set of principal axes bears no obvious relationship to the local distortions at the rare earth site, an unusual site of twelve-fold oxygen coordination.

The second order terms may be also written in less conventional but perhaps more informative form as

$$V_2 = D_1 S_1^2 + D_2 S_2^2 + D_c S_c^2, \qquad \text{V-5}$$

where the D_i have the values

$D_1 = -0.57$ Koe.

$D_2 = +0.47$ Koe. V-6

$D_c = +0.10$ Koe.

If we turn our attention now to the biquadratic term in the spin Hamiltonian V_4, we find a much more complicated situation than we found for the Fe^{3+} spectrum.

The planes in which data were taken are principal planes of the coordination cube of the undistorted site. If the site symmetry remained essentially cubic in the actual crystal, the variation of A_4^o with θ could be represented entirely by a $\cos(4\theta)$ function in both planes. Inspection of the data on $A_4^o(\theta)$ shows this to be far from the actual case; the dominant θ dependence in both planes is a $\cos(2\theta)$ dependence. Therefore we cannot make the simplifying assumption that the fourth order potential has cubic symmetry and that one field magnitude parameter is sufficient to characterize the potential. Fortunately, the nine general coefficients of the V_4 potential are reduced to five by the mirror plane symmetry of the rare earth site (all $Y_4^{\pm m}$ are eliminated for which m is odd). V_4 can therefore be written

$$V_4(\vec{\alpha}) = A(35\alpha_3^4 - 30\alpha_3^2 + 3) + 4B(\alpha_1^2 - \alpha_2^2)(7\alpha_3^2 - 1)$$
$$+8C\alpha_1\alpha_2(7\alpha_3^2 - 1) + 2D(\alpha_1^4 + \alpha_2^4 - 6\alpha_1^2\alpha_2^2) \qquad \text{V-7}$$
$$+8E\alpha_1\alpha_2(\alpha_1^2 - \alpha_2^2).$$

By use of the operator equivalents of Table IV-1 we have the fourth order part of the spin Hamiltonian

$$V_4(\vec{S}) = A\left[35S_3^4 - 30S(S+1)S_3^2 + 25S_3^2 - 6S(S+1)+3S^2(S+1)^2\right]$$

$$+B\left\{(S_+^2 + S_-^2)\left[7S_3^2 - S(S+1) - 5\right] + \left[7S_3^2 - S(S+1)-5\right](S_+^2 + S_-^2)\right\}$$

$$-iC\left\{(S_+^2 - S_-^2)\left[7S_3^2 - S(S+1)-5\right] + \left[7S_3^2-S(S+1)-5\right](S_+^2 - S_-^2)\right\} \qquad \text{V-8}$$

$$+ D\left[S_+^4 + S_-^4\right] - iE\left[S_+^4 - S_-^4\right],$$

where $S_{\pm} = S_1 \pm S_2$. For H_o in the a-b plane $\alpha_3 = 0$, $\alpha_1 = \cos\phi$ and $\alpha_2 = \sin\phi$, where ϕ is the angle between H_o and the a axis. Therefore, for H_o in the a-b plane

$$V_4 = A_4^o/15 = A - 4B\cos 2\phi - 4c \sin 2\phi + 2D\cos 4\phi + 2E \sin 4\phi \,. \qquad \text{V-9}$$

Similarly, for H_o in the b-c plane, $\alpha_3 = \cos\theta$, $\alpha_2 = \sin\theta$, $\alpha_1 = 0$ and in this plane

$$V_4 = A_4^o/15 = \frac{3}{8}(3A-4B+2D) + (\frac{5}{2}A-2B-D)\cos 2\theta$$

$$+(\frac{35}{8}A + 7/2B + 1/4D)\cos 4\theta. \qquad \text{V-10}$$

The best fit obtained between these expressions and the data of Fig. 13 was obtained for

$$A = -0.35 \text{ oe.}$$

$$B = -0.21 \text{ oe.}$$

$$C = -0.98 \text{ oe.} \qquad \text{V-11}$$

$$D = +0.53 \text{ oe.}$$

$$E = -0.59 \text{ oe.}$$

The curves calculated from these values are plotted in Fig. 12 along with the data. The fit is fair or good, but not excellent. It should be noted that the data may contain considerable systematic error, since the A_4^o points were calculated from smoothed curves drawn through the raw data. The A_4^o are small quantities, on the order of 10 gauss, obtained from the subtraction of nearly equal resonance fields of the order of 10^4 gauss, thus magnifying any systematic error.

The spin Hamiltonian coefficients A through E as deduced for the Gd^{3+} site above describe a potential which is very far from cubic. For a cubic potential at this site B, C and E would be zero, whereas in fact C is the largest coefficient obtained, and E is the next largest. Further, for a cubic site D = -5A/2, a relationship also violated in the Gd^{3+} data fit. In short, the paramagnetic resonance results on Gd^{3+} indicate that the rare earth ion site in the orthoaluminate is so severely distorted from the cubic prototype that no visible cubicity remains. Calculations of crystal field effects based on a cubic approximation would appear invalid.

VI. CRYSTAL FIELD CALCULATIONS.

A. The Iron Site.

The dominant crystal field effect on an S state ion like Fe^{3+} is usually quadratic in the spin components. This quadratic form can always be diagonalized by a proper rotation of coordinates and the direction of the principal axes and their magnitudes specified. The resolution of the resonance data in section IV has given us the orientation and shape of the quadratic energy tensor for Fe^{3+} in $YAlO_3$.

We now proceed to calculate the crystalline electric fields present in the orthoferrite on a point ion model and compare these with the data. Since the mechanism connecting the coefficients in the spin Hamiltonian and the crystal fields actually present is not understood quantitatively for S state ions, we cannot pursue a truly quantitative comparison. We can, however, calculate the quadratic (in coordinates) part of the crystal field at the iron site on a point ion model and compare the orientation and shape of this quadratic form with the experimentally determined spin Hamiltonian.

The iron ion occupies in the orthoferrite a position of sixfold oxygen coordination, as illustrated in Fig. 13. The distortion of the coordination octahedron from a purely cubic configuration is substantial. At present we have the oxygen parameters only for $GdFeO_3$;[6] those for $YAlO_3$, really appropriate for this calculation, are currently being determined by Dr. Ferdinand Euler at Air Force Cambridge Research Center. Since the $GdFeO_3$ parameters are the only ones available we shall therefore

proceed using them. They give us the following radius vectors, in Å, from the Fe^{3+} ion at special position (1/2, 0, 0) to nearest neighbor oxygens:

$$\vec{r}_1 = 1.94\ (-.139\vec{i} - .088\vec{j} + .990\vec{k})$$

$$\vec{r}_2 = 1.94\ (+.139\vec{i} + .088\vec{j} - .990\vec{k})$$

$$\vec{r}_3 = 2.03\ (-.772\vec{i} + .620\vec{j} - .187\vec{k})$$

$$\vec{r}_4 = 2.03\ (+.772\vec{i} + .620\vec{j} + .187\vec{k}) \qquad \text{VI-1}$$

$$\vec{r}_5 = 1.94\ (-.577\vec{i} - .794\vec{j} - .196\vec{k})$$

$$\vec{r}_6 = 1.94\ (+.577\vec{i} + .794\vec{j} + .196\vec{k})$$

where $\vec{i}$, $\vec{j}$ and $\vec{k}$ are unit vectors in the unit cell a, b and c directions respectively, and the oxygens are indexed according to the scheme illustrated in Fig. 13. The potential at a point $R\theta\phi$ within the coordination cube can be expressed as[33]

$$V = e^2 \sum_{i=1}^{6} \sum_{n=0}^{\infty} \sum_{m=-n}^{m=+n} \frac{4\pi}{2n+1} \frac{Z_i R^n}{r^{n+1}} Y_n^m(\theta_i \phi_i) Y_n^m(\theta, \phi) \qquad \text{VI-2}$$

where the Y_n^m are spherical harmonics, the summation over i is, in this case, over the oxygen neighbors, and the $r_i \theta_i \phi_i$ are the spherical coordinates of the neighbors. For the present we are concentrating on the quadratic portion of the potential, that corresponding to n = 2. Performing the indicated summations for n = 2 one obtains the potential

$$V(2) = V_o R^2 \left(\frac{4\pi}{5}\right)^{1/2} \left[5.1\, Y_2^{\,o} + \frac{1}{\sqrt{6}}(8.4 - i\,2.6) Y_2^{+1}\right.$$

$$+ \frac{1}{\sqrt{6}}(8.4+i\,2.6) Y_2^{-1} + \frac{1}{\sqrt{6}}(-4.3+i\,4.2)\, Y_2^{+2} \qquad \text{VI-3}$$

$$\left. + \frac{1}{\sqrt{6}}(-4.3 - i\,4.2) Y_2^{-2}\right].$$

Several proportionality constants have been absorbed into V_o, but its exact definition is not important here since we wish to examine only the location and relative sizes of the principal axes of the form. To accomplish the diagonalization the potential was first put into the coordinate form:

$$V(2) = V_o \left[-4.70\, x^2 - 0.40\, y^2 + 5.10\, z^2\right.$$

$$\left. -4.20\, xy + 2.60\, yz + 8.40\, xz\right]. \qquad \text{VI-4}$$

The transformation T was then sought which diagonalized the quadratic form; this same transformation yields the directional cosines of the principal axes of the form. The desired transformation is:

$$\begin{pmatrix} x' \\ y' \\ z' \end{pmatrix} = \begin{pmatrix} .875 & -.343 & -.343 \\ .324 & .944 & -.069 \\ .339 & -.046 & .938 \end{pmatrix} \begin{pmatrix} x \\ y \\ z \end{pmatrix} \qquad \text{VI-5}$$

and the principal values are

$$\lambda(x') = -7.08$$

$$\lambda(y') = 0.41 \qquad \text{VI-6}$$

$$\lambda(z') = 6.67$$

Let us now compare these results with our spin Hamiltonian, whose principal values were $D_3 = -1.45$, $D_2 = 0.27$, $D_1 = 1.18$. Superficially these are similar, one large negative value, one positive value almost as large, and one small positive value. Correlation ceases at this point, however. The principal axes of the two tensors bear little relation to one another. Only one close correlation exists, in that the D_3 axis of the spin Hamiltonian is close to the y' axis of the point ion potential, but this is at best an unfortunate correlation, since D_3 is associated with the large negative principal value whereas y' is associated with the small positive principal value.

A very likely source of this lack of correlation is the circumstance that calculations based on the oxygen coordinates for the $GdFeO_3$ are used to compare with data taken on $YAlO_3$. It has been shown by other investigators that the quadratic potential is particularly sensitive to crystalline distortions. Remai and deMars,[35] in a study of the paramagnetic resonance spectrum of Gd^{3+} in gallium and aluminum garnets, showed that the second order potential coefficients changed by factors of from two to four in going from YGaG to YAlG, while the fourth order potential coefficients were changing 5 to 10 percent. Only further work, using the positional parameters appropriate for $YAlO_3$ can resolve this question.

B. <u>The Rare Earth Ion Site.</u>

The rare earth ions in the orthoferrite occupy an unusual site with twelve nearest neighbor oxygens, which may be visualized as occupying

the midpoints of the twelve edges of a cube surrounding the rare earth site. The eight corners of the cube are occupied by trivalent cations, Fe^{3+} in $YFeO_3$, or Al^{3+} in $YAlO_3$. In the orthorhombically distorted perovskite the cation cube remains rigorously cubic, but the rare earth ion is displaced (in the a-b plane) from the center of this cube and the oxygens are displaced from their positions at the midpoints of the cube edges.

We have not calculated the crystal fields at the rare earth ion for the distorted perovskite. The results of the immediately previous section indicate strongly that the positional parameters obtained from $GdFeO_3$ do not yield useful potentials for interpreting the data on $YAlO_3$. We have, however, made some crystal field calculations in the cubic approximation, primarily to establish an expected sequence of energy levels for the Yb^{3+} optical studies. The potential was calculated from expression VI-2, with the summation in i now running over the twelve oxygen neighbors. The resulting potential is

$$V = C_4 \left\{ -\frac{7}{4} Y_4^{\circ}(\theta\phi) - \sqrt{\frac{70}{8}} \left[Y_4^{+4}(\theta\phi) + Y_4^{-4}(\theta\phi) \right] \right\} + \frac{39}{16} C_6 \left\{ -V_6^{\circ}(\theta\phi) + \sqrt{14} \left[Y_6^{+4}(\theta\phi) + Y_6^{-4}(\theta\phi) \right] \right\}, \qquad \text{VI-7}$$

where

$$C_4 = \left(\frac{4\pi}{9}\right)^{1/2} \frac{Ze^2R^4}{a^5}$$

$$C_6 = \left(\frac{4\pi}{13}\right)^{1/2} \frac{Ze^2R^6}{a^7} \qquad \text{VI-8}$$

We may compare this with the cubic potentials for the four, six, and eightfold coordinated site, as calculated, say, by Wolf, et al.[36] We find that the coefficients of the Y_4^o and Y_6^o terms are of the same relative sign, as in the case for the octahedral (six-fold coordinated) site, but that the signs of both the Y_4^o coefficient and the Y_6^o coefficient are opposite for the 12 fold site from what they were for the six fold site. We therefore expect that the crystal field splitting of any particular J state of a given ion will be inverted in the twelvefold case as compared to the six fold case. Specifically, we expect that the excited J = 5/2 state of the Yb^{3+} ion in the orthoferrite will have the Γ_8 quartet lowest and the Γ_7 doublet higher; and that for the J = 7/2 ground state either the Γ_8 quartet or the Γ_7 doublet may be lowest.

Referring to Fig. 14 we observe that the doublet state (Γ_7 ?) lies lower than the quartet (Γ_8 ?) for the J = 5/2 state of Yb^{3+}, in direct contradiction to the predictions of the preceding paragraph.

The crystal field splitting of the J = 5/2 state depends, in the cubic approximation, only on V_4, the fourth order term in the crystal field potential. The Γ_7 doublet can be lowest only if the sign of the coefficient of V_4^o is positive. To see if the neglect of next-to-nearest, etc. neighbors could be affecting the sign of V_4^o we have carried this part of the calculation out to fourth nearest neighbors, with the results shown in Table VI-1. The coefficient of V_4^o remains negative at all times,

Neighbor	Radius	Contribution to potential	Cumulative total potential
12 O^{2-}	a	$-3.5\ \frac{e^2R^4}{a^5}$	$-3.5\ e^2R^4/a^5$
8 Al^{3+}	$a\sqrt{3/2}$	$+3.39\ \frac{e^2R^4}{a^5}$	$-.11\ e^2R^4/a^5$
6 Y^{3+}	$a\sqrt{2}$	$-1.86e^2R^4/a^5$	$-1.97e^2R^4/a^5$
24 O^{2-}	$a\sqrt{3}$	$-.45e^2R^4/a^5$	$-2.42e^2R^4/a^5$

TABLE VI-1

and converges on a negative value not too different from the nearest neighbor only coefficient.

We cannot get the correct sequence of levels for the 5/2 state unless we abandon the cubic approximation, a result we have already anticipated from the Gd^{3+} spin Hamiltonian.

VII. ABSORPTION SPECTRUM OF Yb^{3+}

A. Optical.

The absorption spectrum of Yb^{3+} in the near infrared was studied at high resolution and at low temperatures (down to 4.2° K). The absorption was studied both for Yb^{3+} dilutely substituted into $YAlO_3$ and for the fully substituted $YbFeO_3$. It was anticipated that an understanding of the crystal fields present would be obtained, and that direct observations of the Yb^{3+} - Fe^{3+} exchange [37-39] would be made.

Unfortunately, though interesting and suggestive data has been obtained, the objectives have been attained in only a limited degree. Considerably more information remains to be uncovered in future spectroscopic work.

Ytterbium, though electronically the simplest of the rare earths substituents in the orthoferrites, does not always exhibit a spectrum which is easily interpreted. First of all there is not enough redundancy in this very sparse spectrum to allow a cross-check of assignments. In addition, the vibrational-electronic interaction is especially strong for ytterbium, and combination (vibronic) lines often rival the pure electronic lines in intensity. This makes the identification of pure electronic levels difficult. Fortunately the vibronic lines are generally somewhat more diffuse than the electronic lines. Furthermore the vibronic lines seem generally to be suppressed in the dilutely-doped crystals. Thus the logical procedure is to identify insofar as possible the pure electronic transitions for Yb dilutely incorporated in $YAlO_3$, and then to

correlate these results with the spectrum of $YbFeO_3$. This procedure also allows one to first examine crystal field effects and then introduce exchange.

If we accept as pure electronic only the strongest or sharpest lines in the spectrum of $(Y_{.995}Yb_{.005})AlO_3$, we obtain the energy level schemes shown in Fig. 14. The spectra are very similar (except for scale) to those observed for Yb^{3+} in the garnet structure, and one is tempted to make the same level assignments, indexed on a cubic scheme. The (nearly) cubic indexing is also suggested by doubling of those states assigned to the Γ_8 representation. That the crystal fields have changed in going from the aluminate to the ferrite is immediately apparent; the upper state (J = 5/2) splitting increases 50 percent, while the $\Gamma_7 \longrightarrow \Gamma_8$ splitting of the J = 7/2 ground state decreases 25 percent.

We have already discussed the problem of reconciling a point ion potential (cubic approximation) to the level sequence of the J = 5/2 state (sec. VI-B). One might take the position that point ion calculations are meaningless, and attempt an empirical fit of V_4 and V_6 to the data. This approach also leads to dilemmas. One finds that to fit the data for both excited and ground states it is necessary to assume (a) that the V_4 potential is much larger than the V_6; (b) that V_6 changes sign in going from the ortho-aluminate to the orthoferrite. Both of these assumptions are unpalatable, based on other experience in rare earth spectra, and one is again driven toward the abandonment of a cubic approximation.

Very interesting, though as yet incomplete, information on the exchange coupling between the Yb^{3+} and its Fe^{3+} neighbors was obtained from the $YbFeO_3$ spectrum. (In the case of the garnets a very full characterization of this exchange was possible[37-39]). The sharpest line in the $YAlO_3$ spectrum (the $\Gamma_7 \longrightarrow \Gamma_7$ transition in Fig. 14) becomes a diffuse doublet in $YbFeO_3$ with a splitting at 78° K of about 6 cm^{-1}. This splitting is insensitive to temperature down to 8° K, at which temperature the moment of $YbFeO_3$ is known[17] to flop from the $\underline{c}$ axis to the $\underline{a}$ axis. Below this temperature a diffuse four line pattern is observed with larger splittings between adjacent lines (8, 11 and 8 cm^{-1}).

No detailed interpretation of the spectrum has yet been made, but a number of observations could be made. The splittings are surprisingly large in view of the fact that the Fe^{3+} spins and the Yb^{3+} spins are constrained by symmetry considerations to be nearly perpendicular to each other. The isotropic part of the rare earth-iron exchange will therefore be ineffective in polarizing the rare earth ions or in producing a Zeeman splitting in the rare earth spectrum. (In $GdFeO_3$, where both Gd^{3+} and Fe^{3+} are nearly isotropic S states, virtually no polarization of the Gd^{3+} is produced[17] and σ_o is the same as for $YFeO_3$ down to 4.2° K) The exchange splitting in the Yb^{3+} spectrum must be accomplished by the antisymmetric part of the Yb-Fe exchange, and this antisymmetric part appears to be nearly as large as the symmetric exchange observed in Yb iron garnet. This is in itself a remarkable conclusion.

One would expect a four line spectrum from the transitions between two Zeeman split doublets, so the presence of only two lines above 8° K might appear puzzling. However, the spectra were taken on as-grown platelets with the light propagating along the c direction. Since this is also the direction (above 8° K) of polarization of the Yb^{3+} ions, and of the effective field polarizing these ions, it is probable that polarization effects eliminated the two π lines and left only the two σ lines. Below 8° the magnetic polarization is in a plane $\perp$ to the c axis and all four components would be observed. Which splittings belong to which doublet could be deduced from the temperature dependence of absorption intensities. Such an intensity study and further polarization studies should be pursued to derive the latent information in the optical spectrum.

B. Paramagnetic Resonance.

Crystals of $YAlO_3$ doped with .5 percent and with 5 percent Yb were examined at 35 kMc and at 9 kMc, for their paramagnetic resonance spectrum. No absorption identifiable as arising from Yb^{3+} were found at magnetic fields up to 20 kilogauss or at temperatures down to 1.4° K, or for a wide range of microwave power levels or field modulation intensities. The spectra of a considerable variety of impurities were found, including Fe^{3+}, Ni^{3+} and Pt in an unidentified valence state.[40] Yb^{3+} was known to be present in the samples from the optical spectra.

The paramagnetic resonance of the ground state doublet of Yb^{3+} in $YAlO_3$ was expected to yield considerable correlative information for interpreting the optical absorption spectrum and for determining the crystal fields present. The lack of a spectrum is quite surprising and strongly suggests that the ground state is such that $\Delta M_J = 1$ transitions between the two partners of the lowest doublet are forbidden. Such can happen, for instance, for an axial field which might put a $J_z = \pm 7/2$ state lowest. It cannot happen for a cubic field. The negative results of the resonance search tend to indicate that the Γ_7 doublet does not lie lowest in the orthoferrite, since the paramagnetic characteristics of this state are well known.[41,42]

It is also possible that variations in the local geometry, due to some defect common in the orthoferrite structure, broadens the paramagnetic resonance so much as to make it unobservable. There is some evidence (satellite lines) in the optical spectra of considerable site irregularity. It is hard to estimate how seriously to take the line-broadening explanation of the negative results.

VII SUMMARY AND CONCLUSIONS.

A number of pieces will have to be fit together before one can understand the macroscopic magnetic properties of the orthoferrites from an atomic point of view. These pieces of information are comprised of knowledge of the low-lying levels of the magnetically active ions, the relationship of these levels to the ion and its crystalline environment, and the interaction between ions.

We have in the course of this contract work assembled a number of these pieces, but far too few to complete the picture; and it would seem that we have also collected some pieces of information belonging to a different puzzle. In particular it has become apparent that much of the detailed information collected in the ortho-aluminate cannot be applied without considerable interpretation to the orthoferrites.

We have accomplished the following:

(1) Characterized the spin configurations allowed in the orthoferrites from magnetic group theory.

(2) Derived the antiferromagnetic resonance frequencies, static, and rf susceptibilities of yttrium orthoferrite.

(3) Measured the paramagnetic resonance spectra of Fe^{3+} and Gd^{3+} in $YAlO_3$.

(4) Developed a powerful method for extracting the spin Hamiltonian for S state ions on sites of low symmetry.

(5) Solved for the spin Hamiltonian of Fe^{3+} and Gd^{3+}, finding that the Fe^{3+} is nearly cubic, but that the rare earth site is so distorted that no cubicity remains.

(6) Concluded from the Fe^{3+} spectrum that single ion anisotropy effects would not be large enough to cause the observed canting in $YFeO_3$.

(7) Compared the spin Hamiltonian of Fe^{3+} in $YAlO_3$ with crystal field calculations based on $GdFeO_3$ oxygen parameters, and found little correlation.

(8) Found on the basis of optical spectroscopy (of Yb^{3+}) that the crystal fields in $YAlO_3$ are substantially different from those in $YbFeO_3$.

(9) Found from optical observations of exchange splittings in $YbFeO_3$ that a strong antisymmetric exchange ($S_1 \times S_2$) exists between the Yb and Fe magnetizations.

(10) Indicated a number of directions for further work which may clear up the questions and contradictions raised by the investigations to date.

REFERENCES

1. S. Geller and E. A. Wood, Acta. Cryst. 9, 563 (1956).
2. S. Geller and V. B. Bala, Acta Cryst. 9, 1019 (1956).
3. M. A. Gilleo, Acta Cryst. 10, 161 (1957).
4. S. Geller, Acta Cryst. 10, 243 (1957).
5. S. Geller, Acta Cryst. 10, 248 (1957).
6. S. Geller, J. Chem. Phys. 24, 1236 (1956).
7. S. Geller, Acta Cryst. 9, 885 (1956).
8. F. Bertaut and F. Forrat, J. Phys. Rad. 17, 129 (1956).
9. E. O. Wollan and W. C. Koehler, Phys. Rev. 100, 545 (1955).
10. J. B. Goodenough, Phys. Rev. 100, 564 (1955).
11. U. H. Bents, Phys. Rev. 106, 225 (1957).
12. W. C. Koehler and E. O. Wollan, J. Chem. Phys. Solids 2, 100 (1957).
13. W. C. Koehler , E. O. Wollan, and M. K. Wilkinson, Phys. Rev. 118, 58 (1960).
14. R. M. Bozorth, Phys. Rev. Lett. 1, 362 (1958).
15. A. J. Heeger, O. Beckman and A. M. Portis, Phys. Rev. 123, 1652 (1961).
16. D. Treves, Phys. Rev. 125, 1843 (1962).
17. R. M. Bozorth, V. Kramer, J. P. Remeika, Phys. Rev. Lett. 1, 3 (1958).
18. M. A. Gilleo, J. Chem. Phys. 24, 1239 (1956).
19. R. Pauthenet and P. Blum, Compt. rend 239, 33 (1954).
20. H. Forestier and G. Guiot-Guillain, Compt. rend 230, 1844 (1950).

21. R. M. Bozorth, H. J. Williams and D. E. Walsh, Phys. Rev. 103, 572 (1956).

22. The general system of exchange interactions upon which this discussion is based was originally presented by L. Neél, Compt. rend. 239, 8 (1954).

23. I. Dzialoshinski, J. Phys. Chem. Solids 4, 241 (1958).

24. T. Moriya, Phys. Rev. 120, 91 (1960).

25. G. F. Herrmann, Resonance and RF Susceptibilities in Orthoferrites, Scientific Report, Contract No. AF 19(628)-387. Electronics Research Directorate, AFCRC.

26. S. F. Foner, private communication.

27. J. P. Remeika, J. Am. Chem. Soc. 78, 4259 (1956).

28. K. W. H. Stevens, Proc. Phys. Soc. A65, 209 (1952).

29. R. J. Elliott and K. W. H. Stevens, Proc. Roy. Soc. A218, 553 (1953).

30. B. R. Judd, Proc. Roy. Soc. A227, 552 (1955).

31. R. J. Elliott and K. W. H. Stevens, Proc. Roy. Soc. A219, 387 (1953).

32. R. J. Elliott and K. W. H. Stevens, Proc. Phys. Soc. A64, 205 (1951); Ibid A64, (1951); Ibid A65, 370 (1952).

33. W. Low, Paramagnetic Resonance in Solids, Academic Press, New York, 1960, especially Chapter II.

34. S. Geschwind, Phys. Rev. 121, 363 (1961).

35. L. Remai and G. A. de Mars, J. Appl. Phys. 33, 1254 (1962).

36. K. R. Lea, M. J. M. Leask and W. P. Wolf, Technical Note No. 9, Contract No. AF 61(052)-125, Electronics Research Directorate, AFCRC.

37. K. A. Wickersheim and R. L. White, Phys. Rev. Letters 4, 123 (1960).

38. K. A. Wickersheim, Phys. Rev. 122, 1376 (1961).

39. K. A. Wickersheim and R. L.White, Phys. Rev. Lett. 8, 483 (1962).

40. S. Geschwind and J. P. Remeika, J. Appl. Phys. 33, 370 (1962).

41. J. W. Carson and R. L. White, J. Appl. Phys. 31, 53S (1960).

42. D. Boakes, G. Garton, D. Ryan and W. P. Wolf, Proc. Roy. Soc. (London) 74, 663 (1959).

LIST OF PERSONNEL CONTRIBUTING TECHNICALLY TO REPORT

J. W. Carson

G. F. Herrmann

R. A. Lefever

M. Mandel

J. Schneider

L. Sobon

R. L. White

K. A. Wickersheim

M. Tinkham - Consultant

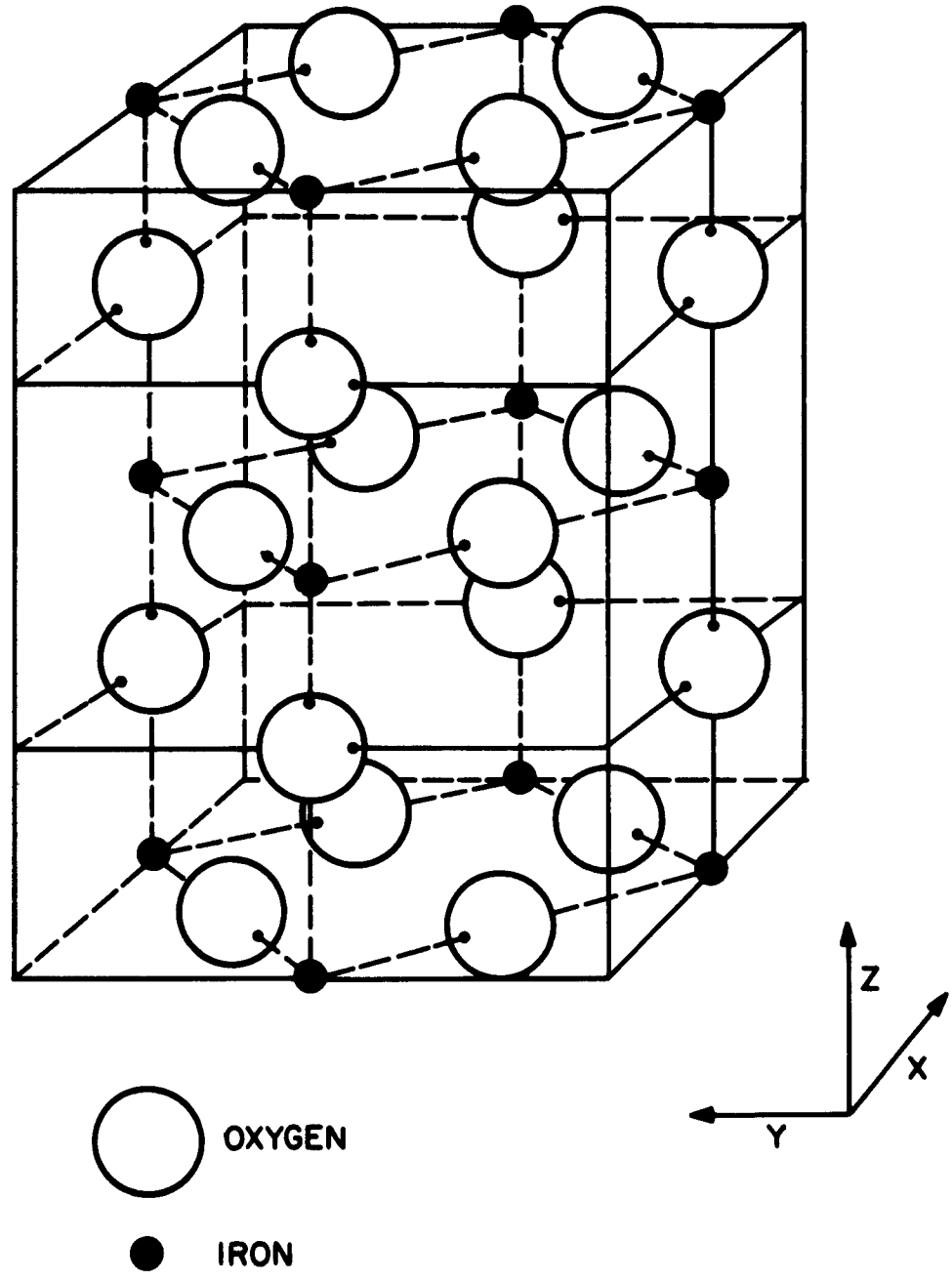

FIGURE 1

Unit cell of the orthorhombic orthoferrite, showing oxygen and iron sites.

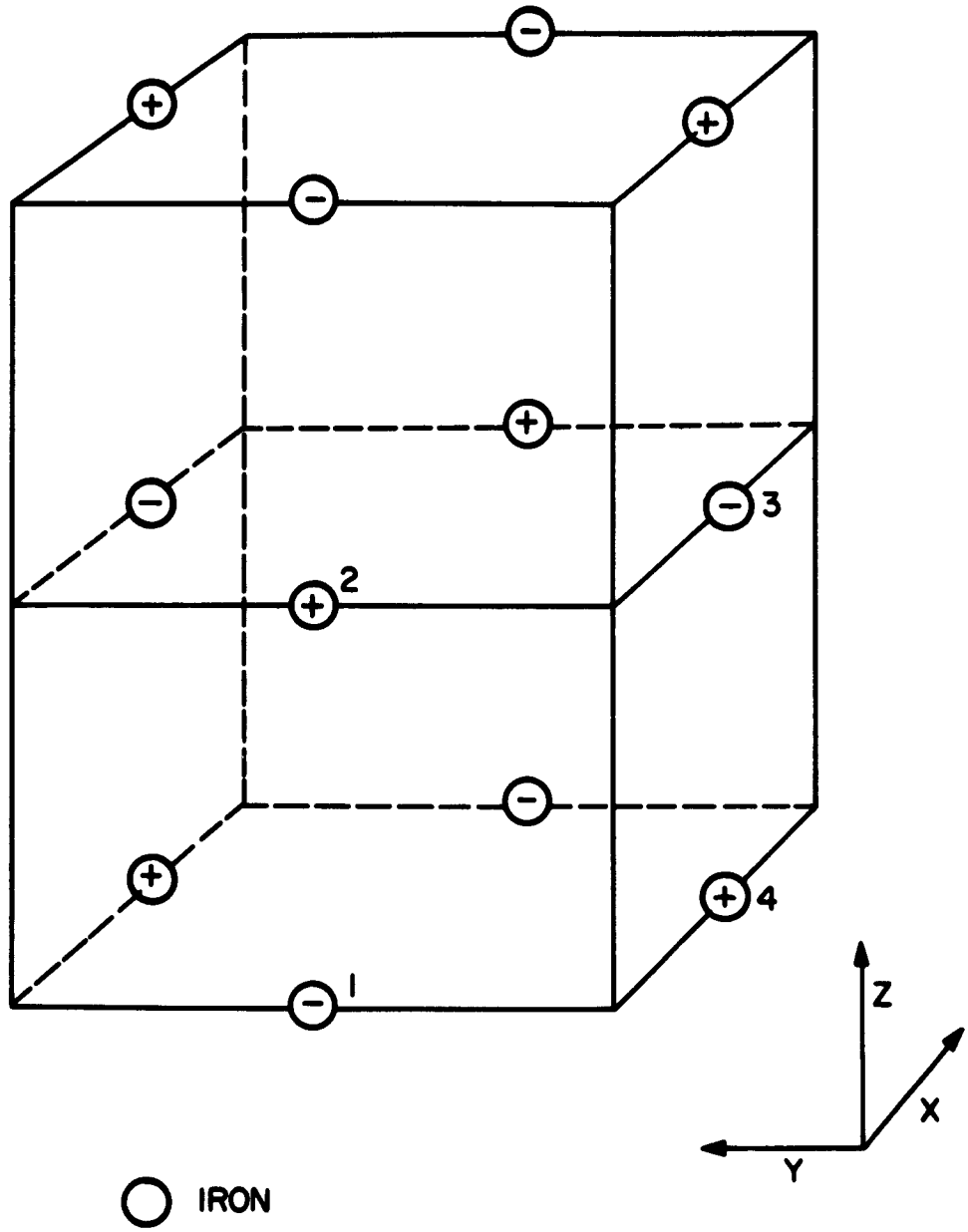

FIGURE 2

Unit cell of the orthorhombic orthoferrite showing and indexing the iron sites.

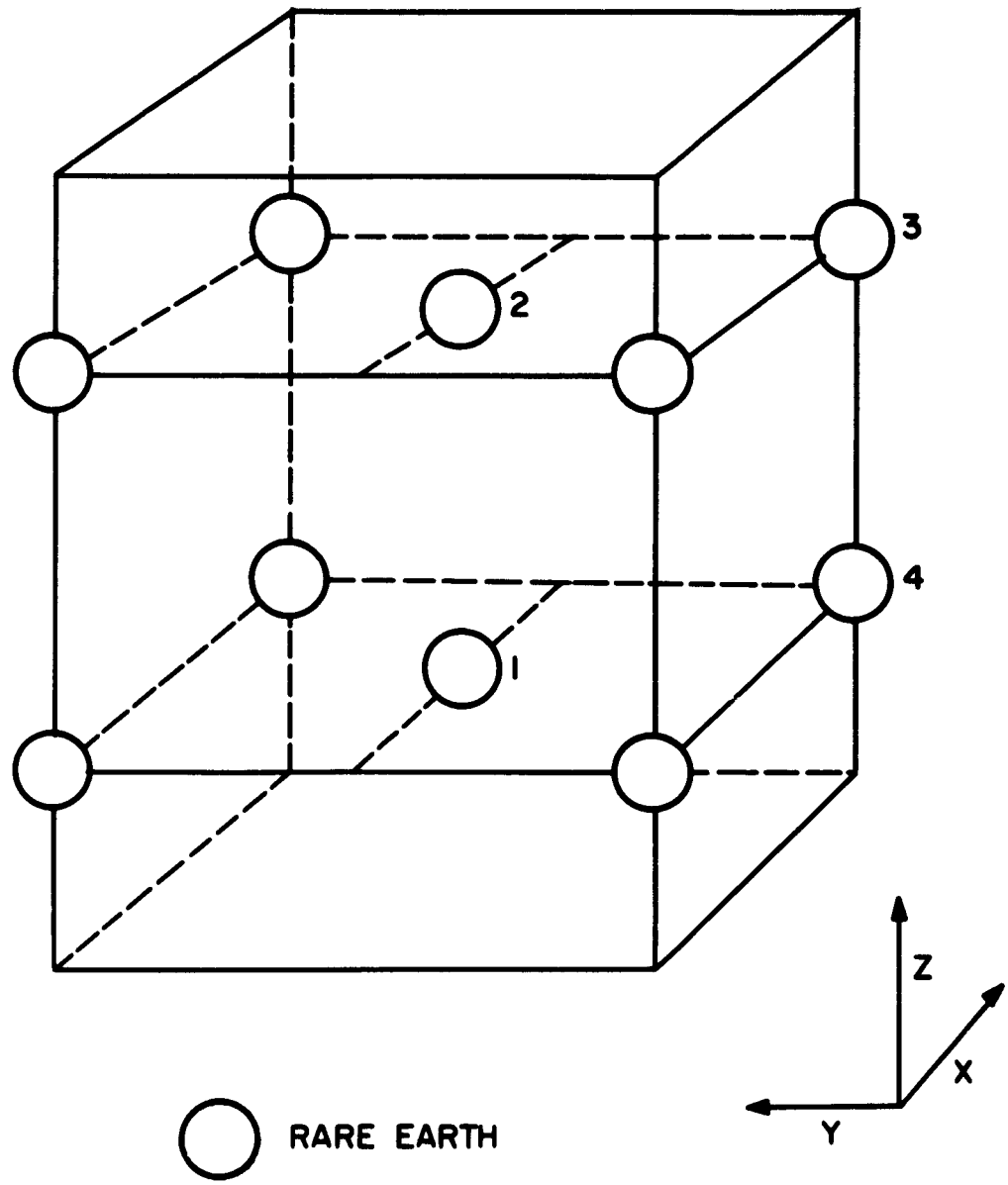

FIGURE 3

Unit cell of the orthorhombic orthoferrite, showing and indexing the rare earth ion sites.

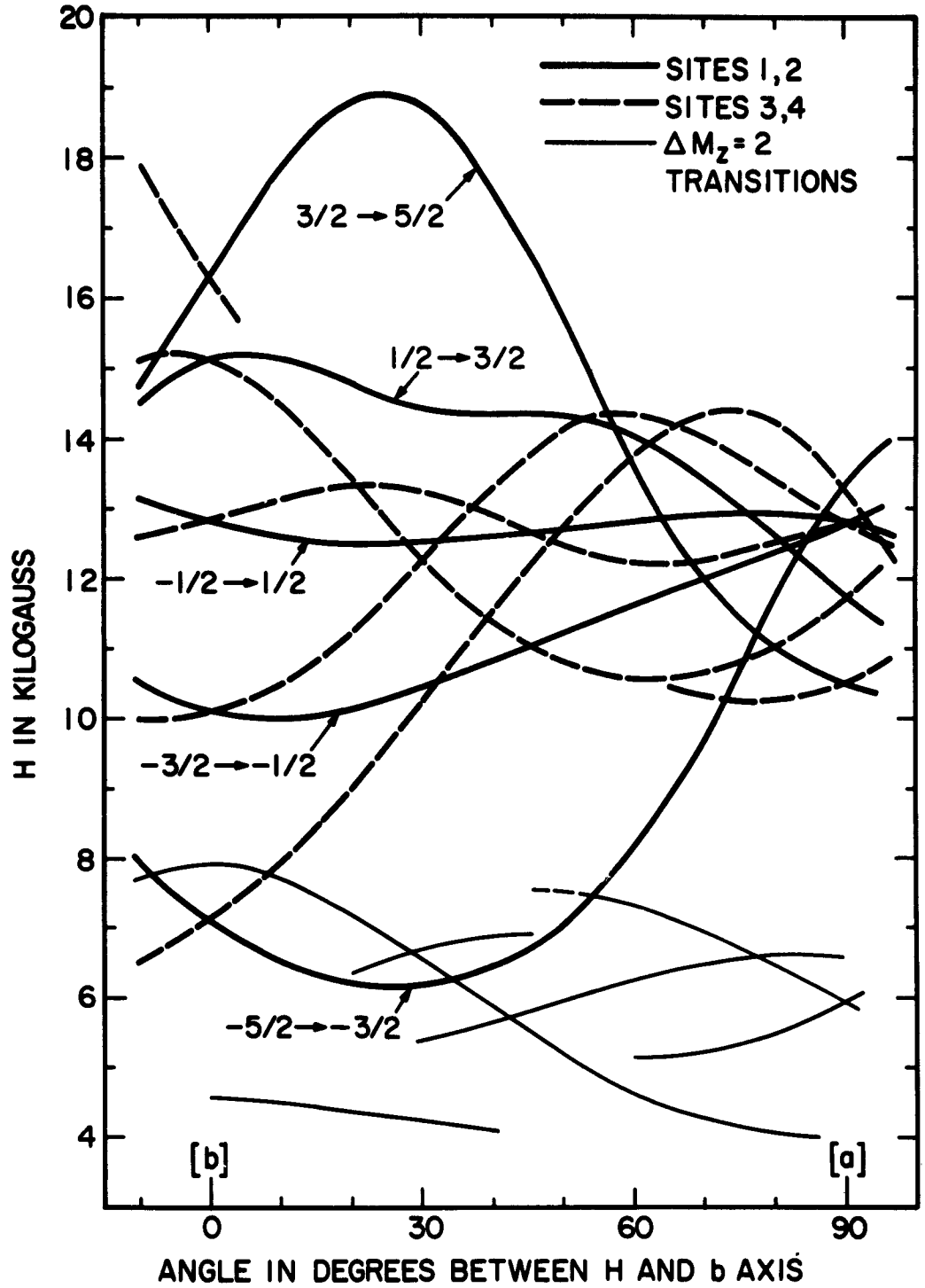

FIGURE 4

Paramagnetic resonance absorption spectrum of Fe^{3+} in $YAlO_3$, with H_o in the a-b plane.

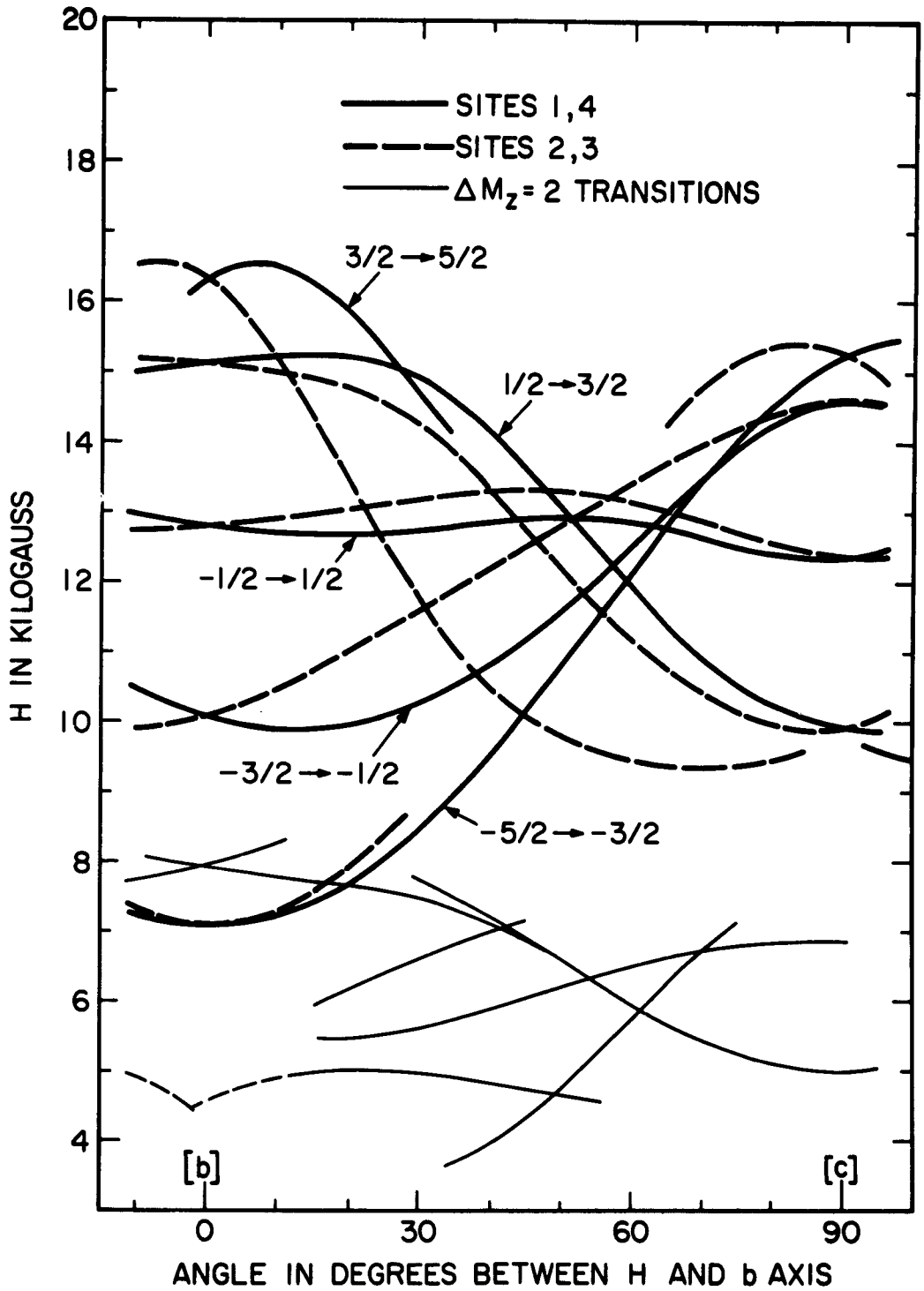

FIGURE 5

Paramagnetic resonance absorption spectrum of Fe^{3+} in $YAlO_3$, with H_o in the b-c plane.

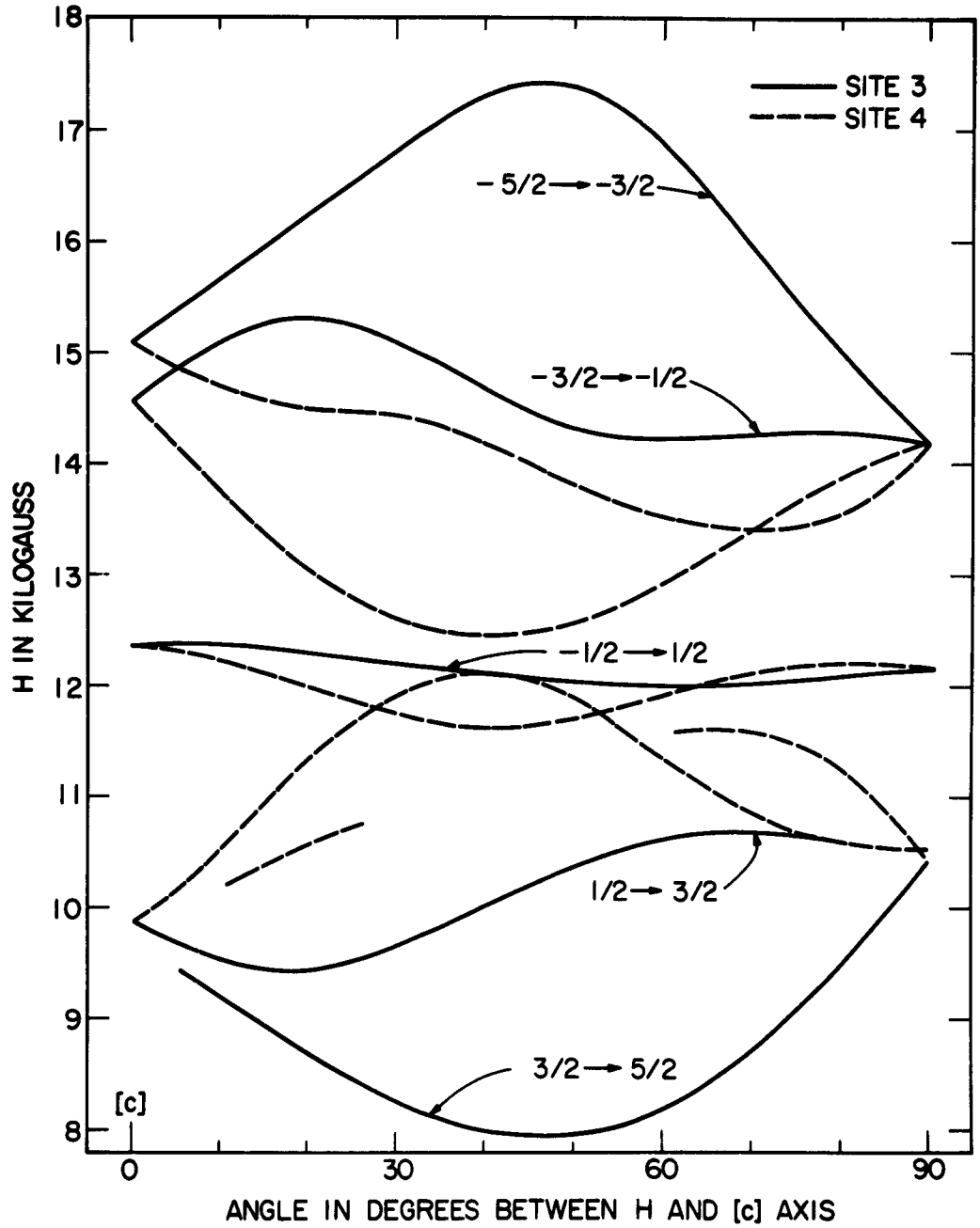

FIGURE 6

Paramagnetic resonance absorption spectrum of Fe^{3+} in $YAlO_3$, with H_o in special plane (see text).

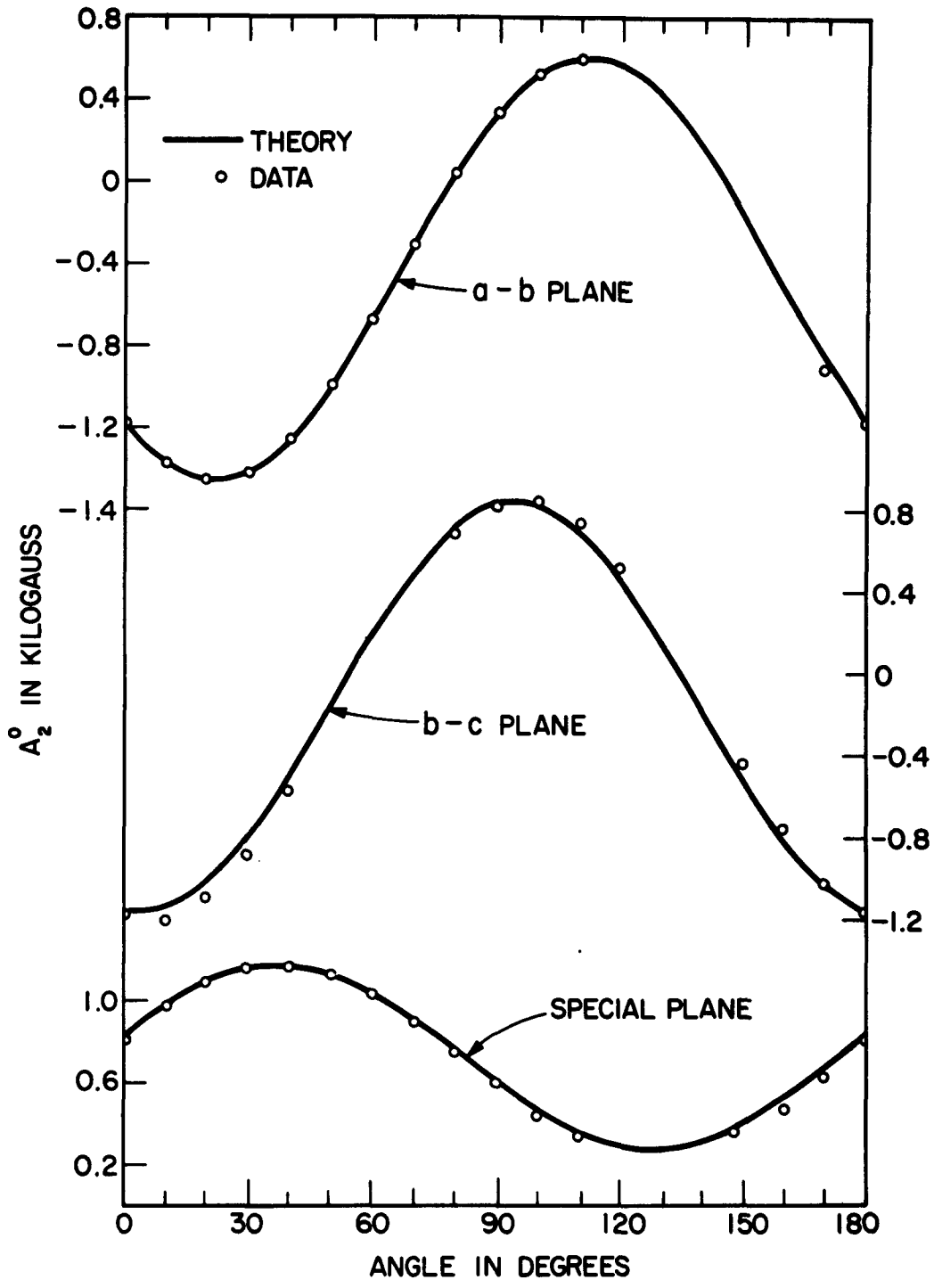

FIGURE 7

Plot of Hamiltonian parameter A_2^o as a function of angle for Fe^{3+} in $YAlO_3$. The angle is measured from the b, b, and c axes in the a-b, b-c and special planes, respectively.

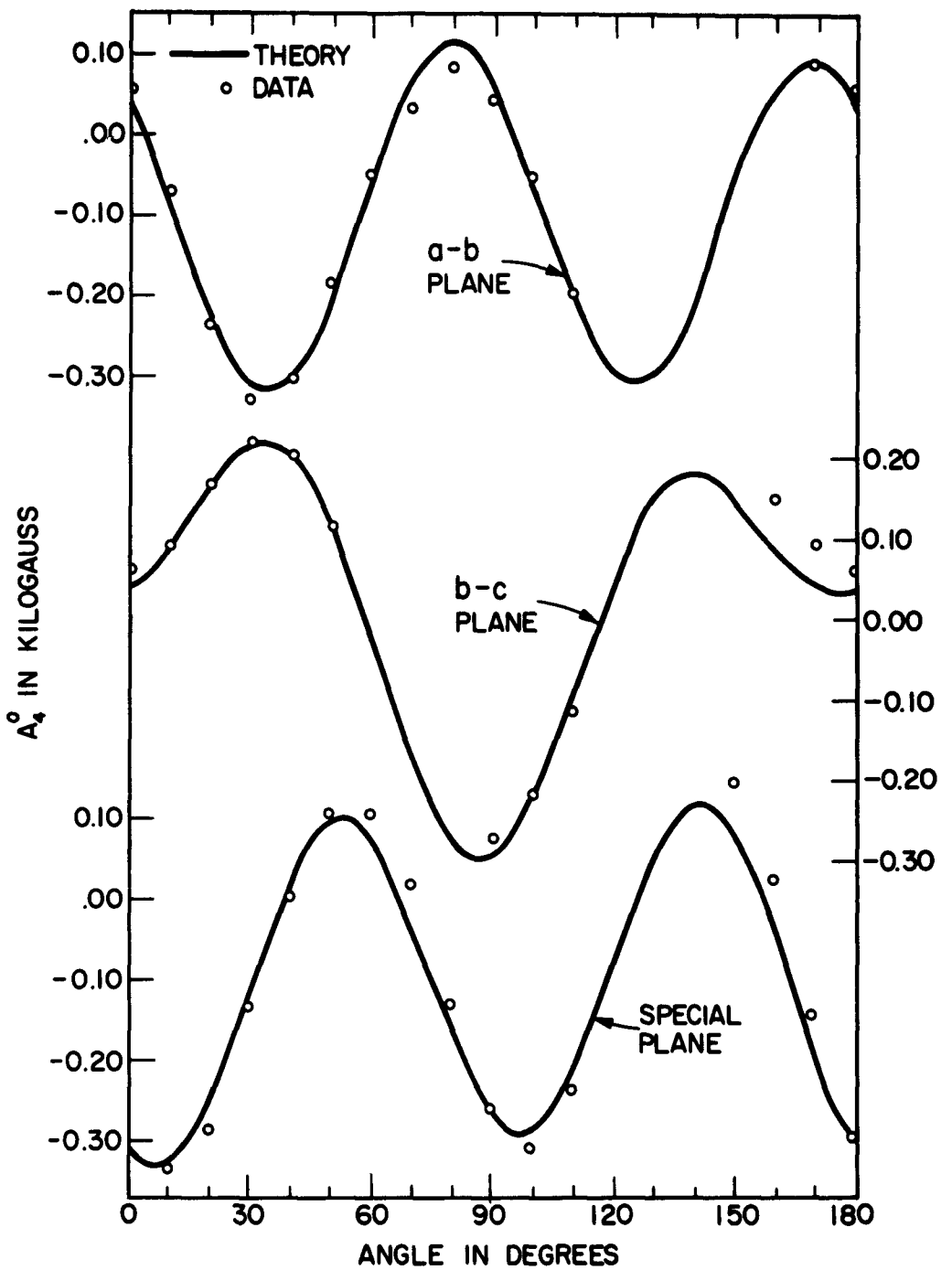

FIGURE 8

Plot of Hamiltonian parameter A_4^0 as a function of angle for Fe^{3+} in $YAlO_3$. The angle is measured from the b, b, and c axes in the a-b, b-c and special cuts respectively.

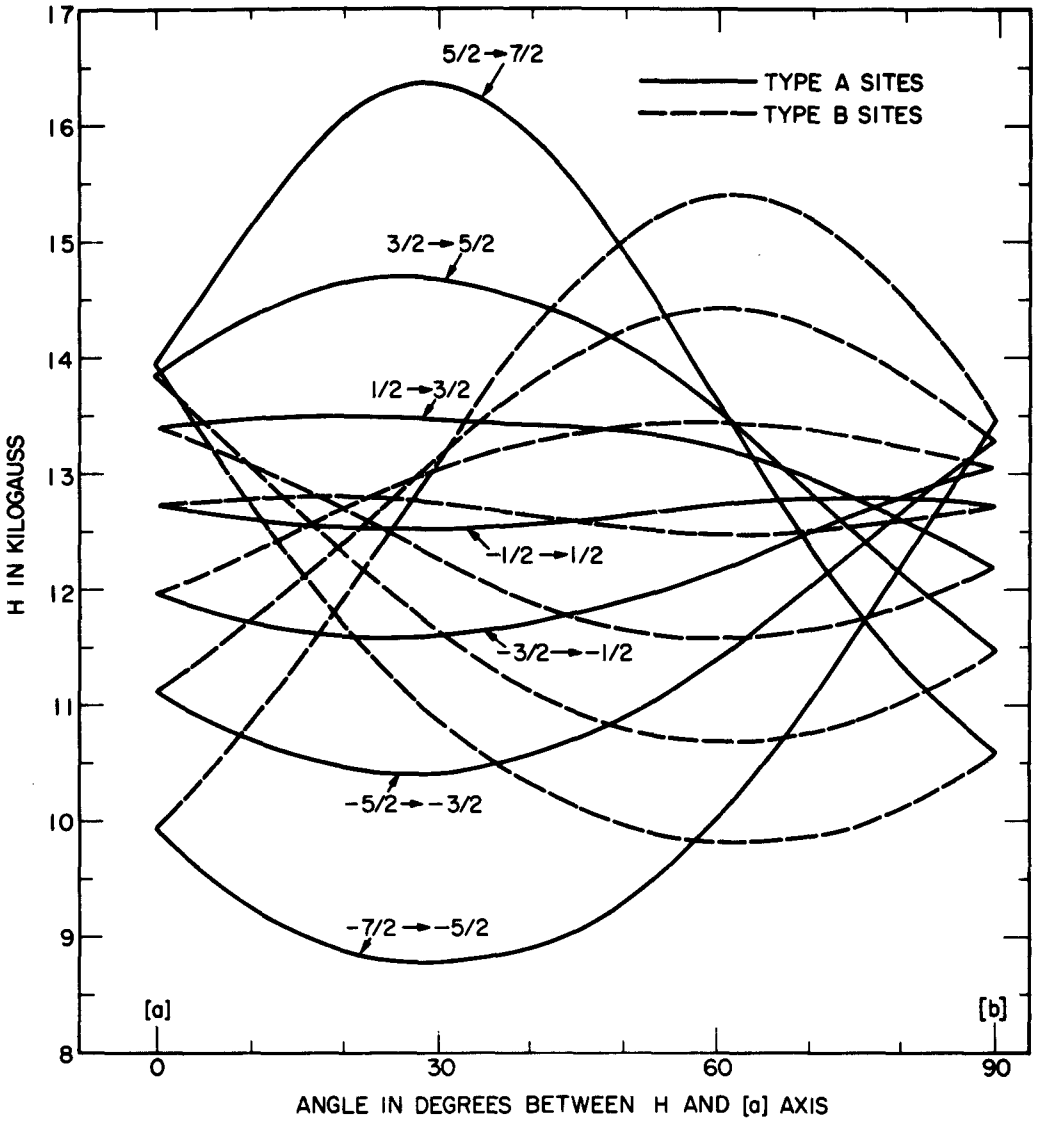

FIGURE 9

Paramagnetic resonance absorption spectrum of Gd^{3+} in $YAlO_3$, with H_o in the a-b plane.

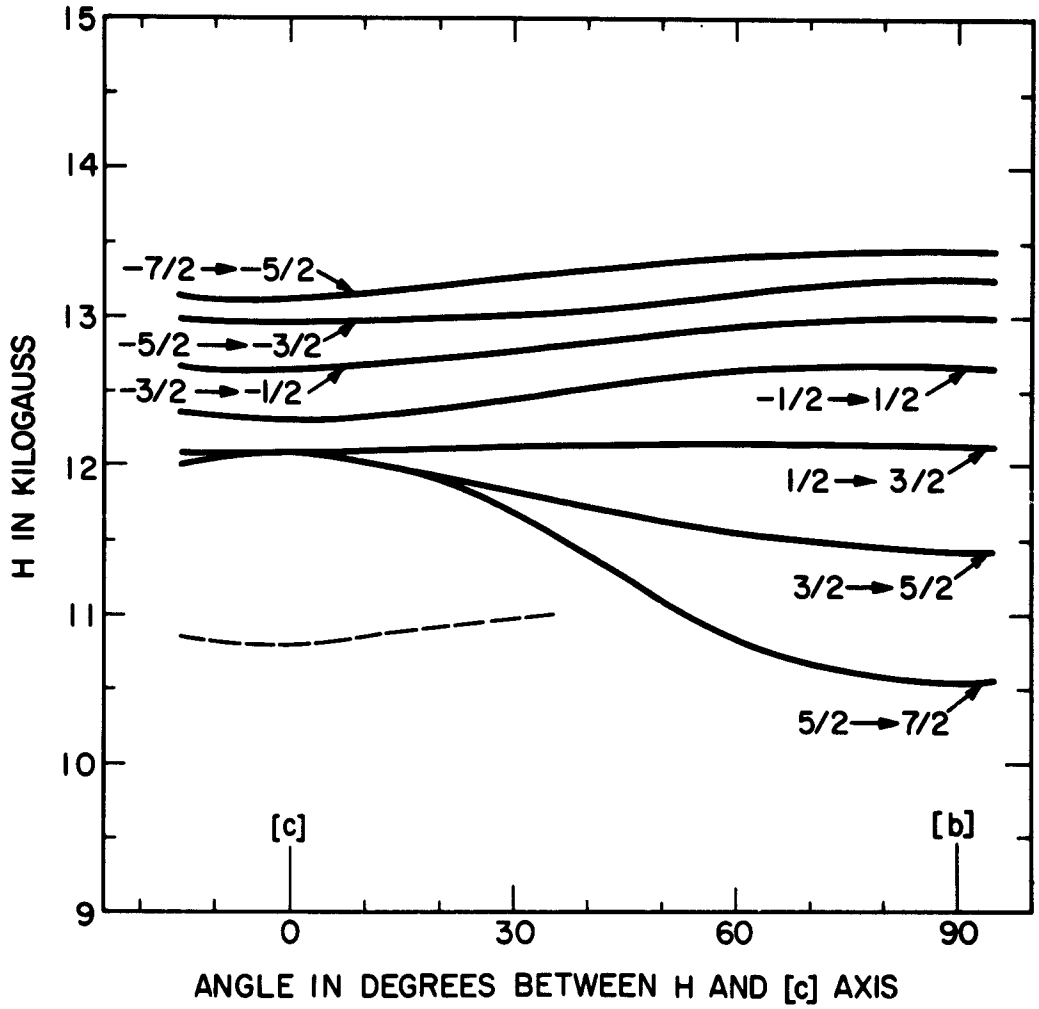

FIGURE 10

Paramagnetic resonance absorption spectrum of Gd^{3+} in $YAlO_3$, with H_o in the b-c plane.

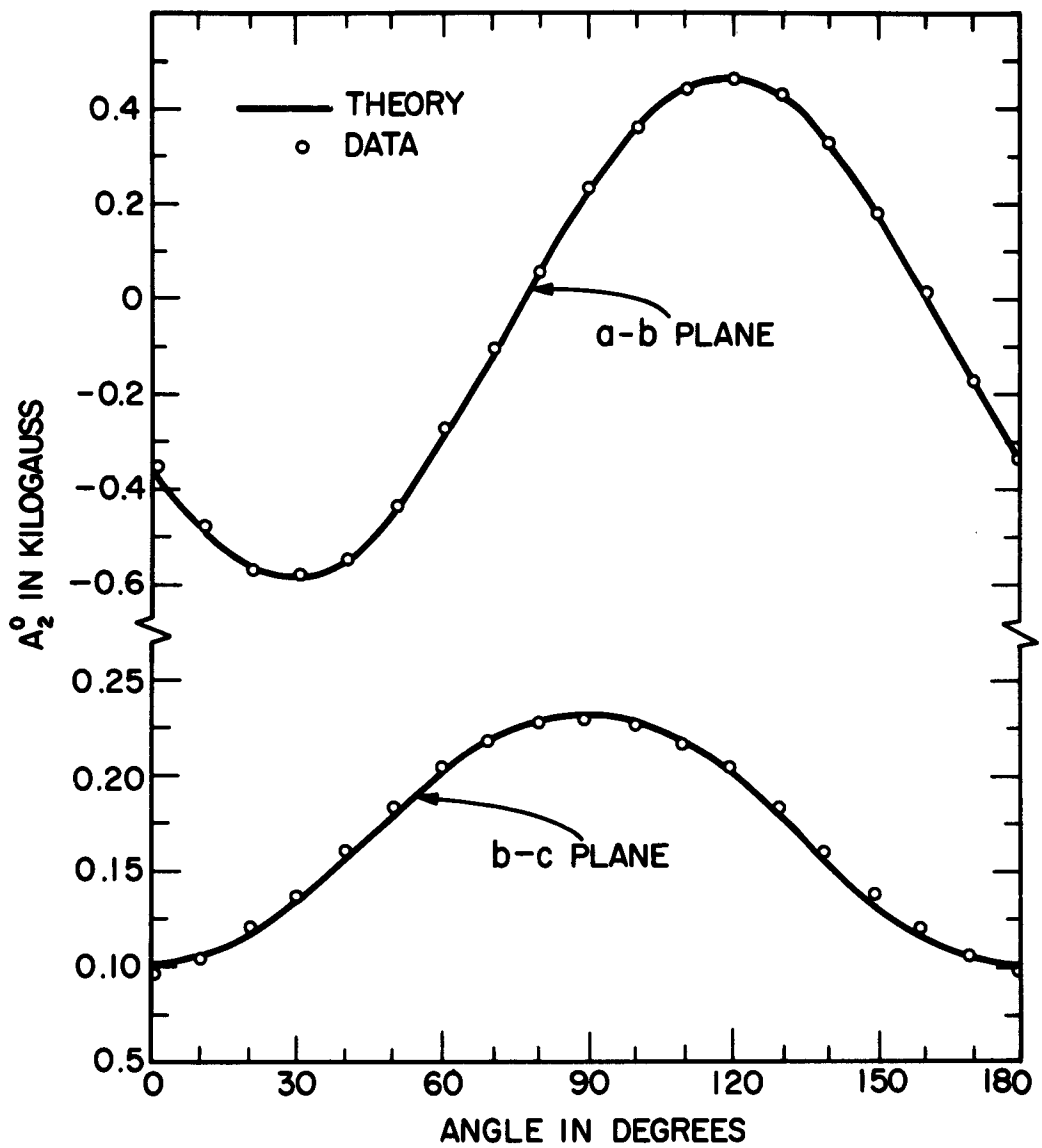

FIGURE 11

Plot of Hamiltonian parameter A_2^o as a function of angle for Gd^{3+} in $YAlO_3$. The angle is measured from the a and c axes in the a-b and b-c planes, respectively.

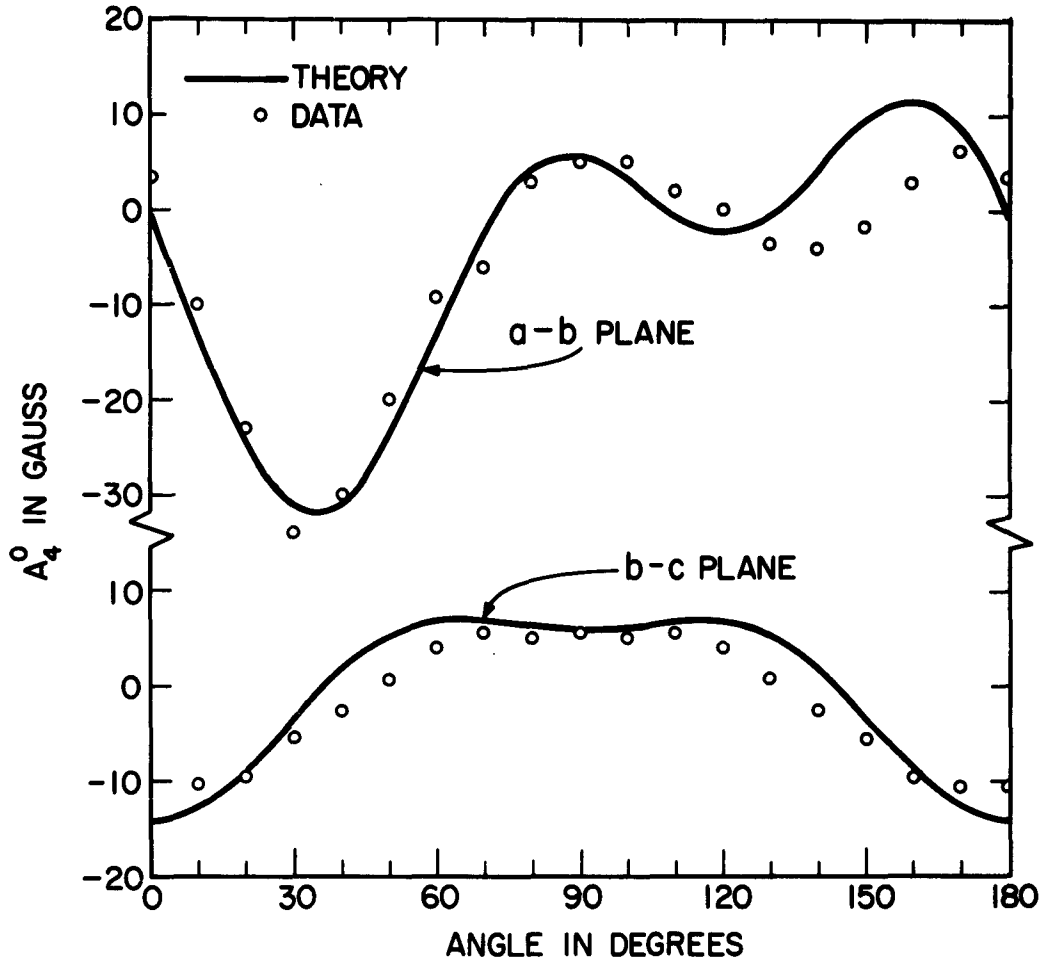

FIGURE 12

Plot of Hamiltonian parameter A_4^o as a function of angle for Gd^{3+} in $YAlO_3$. The angle is measured from the a and c axes in the a-b and b-c planes, respectively.

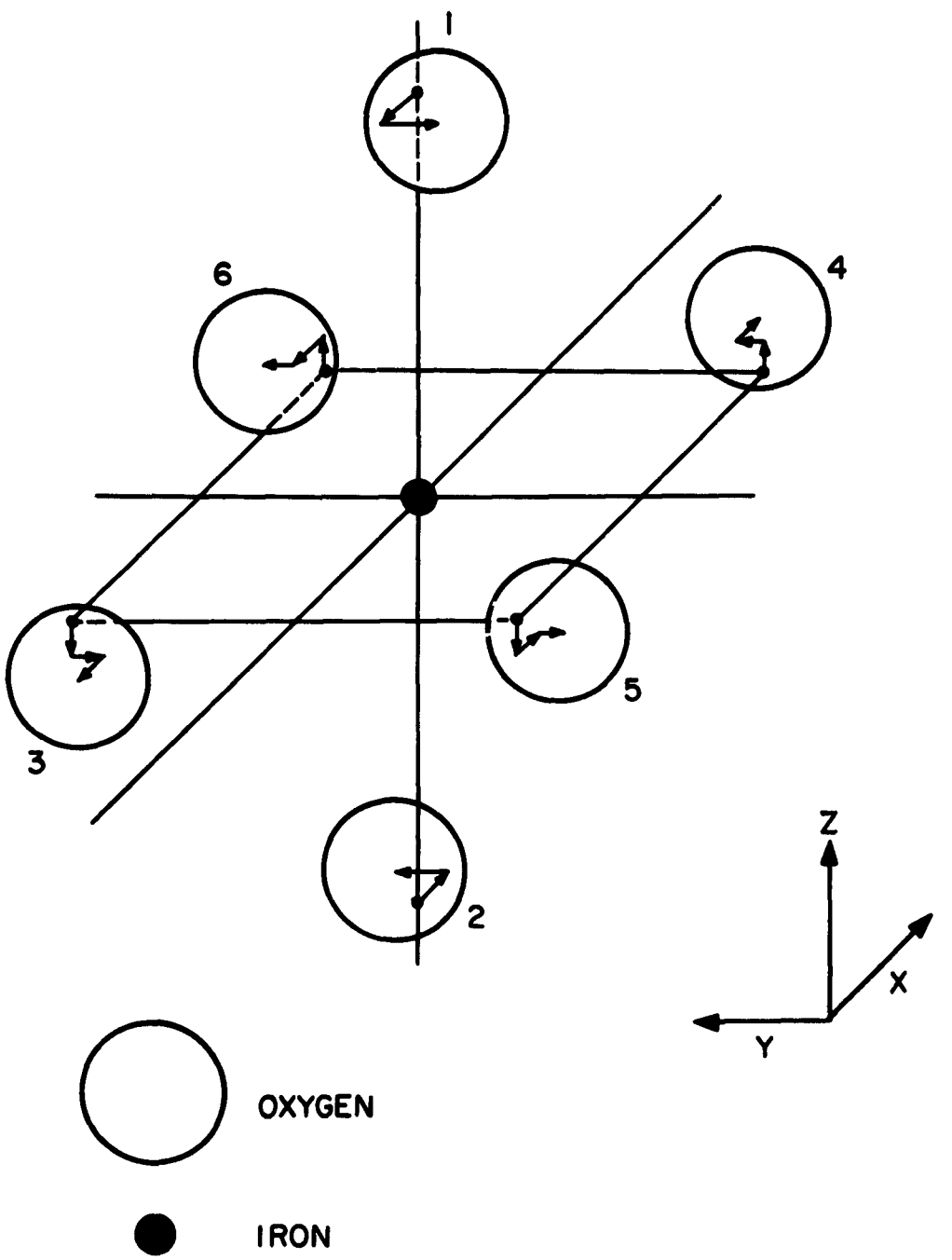

FIGURE 13

Coordination polyhedron for Fe^{3+} in $YAlO_3$, showing the positions of the six nearest neighbor oxygens.

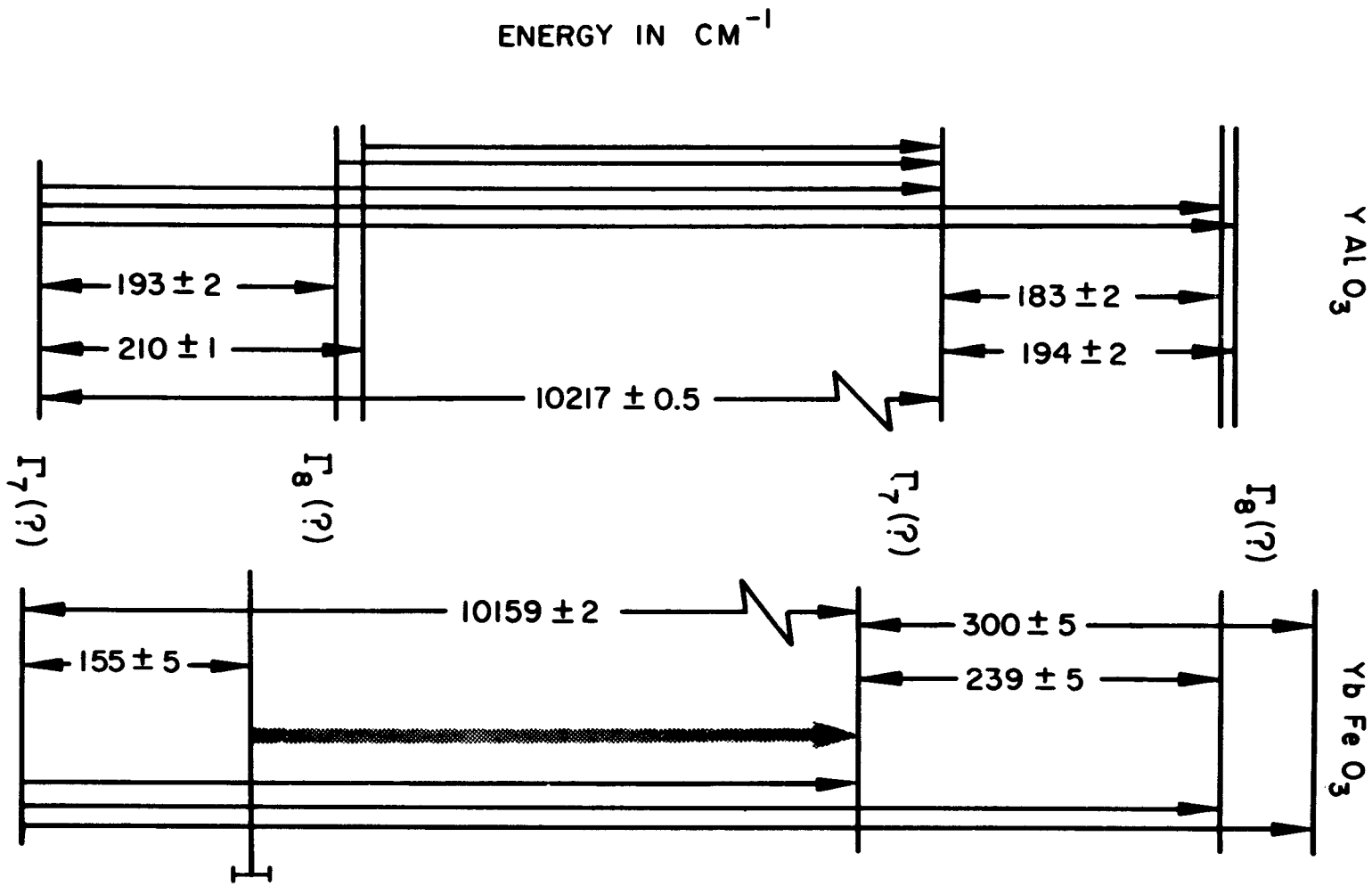

FIGURE 14

Optically determined energy level schemes of Yb^{3+} in $YAlO_3$ and $YbFeO_3$. The transitions observed are indicated at far left and at far right, and an indexing of the levels in a cubic scheme given at the center.

The susceptibilities and antiferromagnetic resonance modes of $YFeO_3$ were calculated. Paramagnetic resonance spectra of Fe^{3+} and Gd^{3+} in $YAlO_3$ were measured and analyzed to give Hamiltonian parameters. Evidence that the crystal fields are substantially different in the orthoaluminates from the orthoferrites were obtained from optical spectra. Large exchange splittings were observed in the optical spectrum of Yb^{3+} in $YbFeO_3$, indicating a large antisymmetric exchange.	I. AFSC Proj. 5621, Task 562104 II. Contract No. AF 19(628)-387 III. G.T. and E. Labs, Microwave Physics Lab., Palo Alto, Calif. IV. White, R. L. V. In ASTIA Collection.	The susceptibilities and antiferromagnetic resonance modes of $YFeO_3$ were calculated. Paramagnetic resonance spectra of Fe^{3+} and Gd^{3+} in $YAlO_3$ were measured and analyzed to give Hamiltonian parameters. Evidence that the crystal fields are substantially different in the orthoaluminates from the orthoferrites were obtained from optical spectra. Large exchange splittings were observed in the optical spectrum of Yb^{3+} in $YbFeO_3$, indicating a large antisymmetric exchange.	I. AFSC Proj. 5621, Task 562104 II. Contract No. AF 19(628)-387 III. G.T. and E. Labs, Microwave Physics Lab., Palo Alto Calif. IV. White, R.L. V. In ASTIA Collection.
The susceptibilities and antiferromagnetic resonance modes of $YFeO_3$ were calculated. Paramagnetic resonance spectra of Fe^{3+} and Gd^{3+} in $YAlO_3$ were measured and analyzed to give Hamiltonian parameters. Evidence that the crystal fields are substantially different in the orthoaluminates from the orthoferrites were obtained from optical spectra. Large exchange splittings were observed in the optical spectrum of Yb^{3+} in $YbFeO_3$, indicating a large antisymmetric exchange.	I. AFSC Proj. 5621 Task 562104 II. Contract No. AF 19(628)-387 III. G.T. and E. Labs, Microwave Physics Lab., Palo Alto, Calif. IV. White, R. L. V. In ASTIA Collection.	The susceptibilities and antiferromagnetic resonance modes of $YFeO_3$ were calculated. Paramagnetic resonance spectra of Fe^{3+} and Gd^{3+} in $YAlO_3$ were measured and analyzed to give Hamiltonian parameters. Evidence that the crystal fields are substantially different in the orthoaluminates from the orthoferrites were obtained from optical spectra. Large exchange splittings were observed in the optical spectrum of Yb^{3+} in $YbFeO_3$, indicating a large antisymmetric exchange.	I. AFSC Proj. 5621, Task 562104 II. Contract No. AF 19(628)-387 III. G. T. and E. Labs, Microwave Physics Lab., Palo Alto Calif. IV. White, R. L. V. In ASTIA Collection.